Mechanisms of ion transport in lithium salt-doped zwitterionic polymer-supported ionic liquid electrolytes *⊗*

Meron Y. Tadesse ⑩ ; Zidan Zhang ⑩ ; Nico Marioni ⑩ ; Everett S. Zofchak ⑩ ; Tyler J. Duncan ⑩ ; Venkat Ganesan □



J. Chem. Phys. 160, 024905 (2024) https://doi.org/10.1063/5.0176149









Mechanisms of ion transport in lithium salt-doped zwitterionic polymer-supported ionic liquid electrolytes

Cite as: J. Chem. Phys. 160, 024905 (2024); doi: 10.1063/5.0176149 Submitted: 11 September 2023 • Accepted: 14 December 2023 • Published Online: 8 January 2024







Meron Y. Tadesse, D Zidan Zhang, Nico Marioni, Everett S. Zofchak, Tyler J. Duncan, Cand Venkat Ganesan

AFFILIATIONS

McKetta Department of Chemical Engineering, University of Texas at Austin, Austin, Texas 78712, USA

a) Author to whom correspondence should be addressed: venkat@che.utexas.edu

ABSTRACT

Recent experimental results have demonstrated that zwitterionic ionogel comprised of polyzwitterion (polyZI)-supported lithium salt-doped ionic liquid exhibits improved conductivities and lithium transference numbers than the salt-doped base ionic liquid electrolyte (ILE). However, the underlying mechanisms of such observations remain unresolved. In this work, we pursued a systematic investigation to understand the impact of the polyZI content and salt concentration on the structural and dynamic properties of the poly(MPC) ionogel of our model polyZI ionogel, poly(2-methacryloyloxyethyl phosphorylcholine) [poly(MPC)] supported LiTFSI/N-butyl-N-methylpyrrolidinium TFSI base ionic liquid electrolyte. Our structural analyses show strong lithium–ZI interaction consistent with the physical network characteristic observed in the experiments. An increase in polyZI content leads to an increased fraction of Li⁺ ions coordinated with the polyZI. In contrast, an increase in salt concentration leads to a decreased fraction of Li⁺ ions coordinated with the polyZI. The diffusivities of the mobile ions in the poly(MPC) ionogel were found to be lower than the base ILE in agreement with experiments at T > 300 K. Analysis of ion transport mechanisms shows that lithium ions within the poly(MPC) ionogel travel via a combination of structural, vehicular diffusion, as well as hopping mechanism. Finally, the conductivity trend crossover between the poly(MPC) ionogel and the base ILE was rationalized via a temperature study that showed that the base ILE ions are influenced more by the variation of temperature when compared to the poly(MPC) ions.

Published under an exclusive license by AIP Publishing. https://doi.org/10.1063/5.0176149

I. INTRODUCTION

The global energy demand is set to reach 660 quadrillion Btu by 2050 increasing by ~15% from 2021.¹ To meet such demands, there has arisen an increasing need for energy storage, conversion materials, and devices.² Lithium (Li)-ion batteries represent one of the most popular renewable energy storage technologies due to their high energy and power density.⁴ Li-ion batteries are typically comprised of some organic solvent electrolyte with a graphite anode and a lithium cobalt oxide (LiCoO₂) cathode material.⁵ It is, however, believed that Li-ion batteries in their present form cannot meet the growing energy demand.⁶ Instead, it has been suggested that the replacement of the graphite anode in Li-ion batteries with a lithium metal anode can potentially increase the theoretical capacity of the battery by approximately tenfold. Although a promising technology, lithium metal batteries are limited by thermal runaway

arising from the growth of dendrites due to the non-homogeneous deposition of lithium metals.⁸ Additionally, lithium metal batteries display electrode corrosion due to their incompatibility with conventionally used organic solvents.⁸ Furthermore, organic solvent electrolytes are also plagued by flammability and volatility. Therefore, there is a strong push for improving electrolyte safety, especially for large-scale energy storage systems.⁵

Ionic liquids (ILs), defined as molten salts with a melting point below 100 °C, play an important role in separations, electrocatalysis, energy applications, etc. ILs have tunable molecular design and exhibit outstanding electrochemical stability and ultralow flammability. Nonvolatile IL-based electrolytes can be designed through the dissolution of salt in the ILs to form what is known as ionic liquid electrolytes (ILEs). As a result, ILEs have attracted interest as alternatives to conventional organic liquid electrolytes. Despite such features, ILs as electrolytes are

challenging to employ, in practice, due to the possibility of leakage. ¹³ Additionally, a significant challenge is to be able to maximize the selective transport of a single target ion, such as Li⁺ or Na⁺, within the extremely ion-dense environment of an ILE, which contains mobile IL anions and cations.

One promising strategy to address the possibility of leakage of liquid electrolytes is through the introduction of a polymer matrix to create what are commonly known as solid polymer electrolytes (SPEs). Polymer electrolytes, such as poly(ethylene oxide) PEO with lithium salt, are well-studied combinations that offer important advantages, such as enhanced mechanical stability. 14,15 More recently, polymerized ionic liquids (PolyILs) have also emerged as alternative solid polymer electrolytes due to the increasing utilization of ionic liquids. 14,16,17 PolyILs are polymers that incorporate repeating units of monomeric IL cation (polycation) or anion (polyanion) depending on the preferred chemical structure. 14,16,17 PolyILs offer a unique combination of properties relating to enhanced safety features from the parent ILs as well as the mechanical stability of solid polymer electrolytes. However, such solid polymer electrolytes are plagued by lower alkali metal transference numbers and conductivities due to the presence of a solid matrix.¹⁵

Recently, polyzwitterionic compounds (polyZIs) are rising as promising candidates for ion gels (ionogels) due to their dual role as mobile ion pair dissociation promoters and as non-covalent crosslinking sites. 11,18,19 PolyZIs are compounds that have an equal number of cationic and anionic portions of charged groups attached to a backbone structure. Although charge-neutral, polyZIs have a large dipole moment and can interact with the ions through their pendant functional groups and/or backbone chemical structure. First pioneered by Ohno and co-workers,²⁰ zwitterions have been used as additives to boost ionic conductivities—a feature that was attributed to their ability to promote ion pair dissociation.²¹ In recent studies, Panzer and co-workers used different polyZI chemistries to immobilize salt-doped IL electrolytes to create ionogel displaying unique properties. 11,18,19 The authors systematically studied three polyZI groups—carboxybetaine (CB), sulfobetaine (SB), and phosphorylcholine (PC)—in various forms inside non-aqueous IL electrolytes to understand their impact on the relative ion interactions and ion transport. 11,18,19 Although the results were dependent on the polyZI, IL, and salt chemistry and compositions, they demonstrated higher ion self-diffusivities and conductivities than the base IL, which highlighted the potential of polyZI for improving the safety and performance of electrolytes.

Other studies such as Keith and Ganesan utilized molecular dynamics (MD) simulations to probe the impact of polyZI architecture on the ion transport characteristics and the mechanism underlying two LiTFSI salt-doped polyZIs of similar composition with different polyZI charge moiety orientations. The authors concluded that the pendant-end counterion displayed higher mobility than the backbone-adjacent counterion across the two different polyZI architectures. In accordance with Keith et al.'s findings, Jones et al. designed a LiTFSI salt-doped IL-inspired zwitterionic polymer [imidazolium-trifluoromethanesulfonamide (Im-TFSI)] with the cation moiety tethered closer to the backbone. The authors reported superionic conductivity measurements despite the sluggish polymer dynamics. Additionally, they demonstrated that the Im-TFSI based polymer electrolyte displayed the presence of ordered and amorphous regions along with two different Li⁺ dynamics

with the fast Li⁺ ions dynamics being an order of magnitude faster than the slower Li⁺ ions.²³ Finally, the Im-TFSI exhibited an improved lithium transport number, which outperformed the traditional upper bound of the polymer electrolyte performance.²³

The present work is motivated by the study of Panzer and co-workers who reported on an ionogel comprised of in situ polymerized polyZI, 2-methacryloyloxyethyl phosphorylcholine [poly(MPC)], in 1 M lithium bis(trifluoromethylsulfonyl)imide (LiTFSI) salt-doped ionic liquid N-butyl-N-methylpyrrolidinium bis(trifluoromethylsulfonyl)imide (BMP TFSI).¹¹ Such an ionogel displayed a surprising result of improved ion transport properties compared to the base ionic liquid electrolyte (ILE), 1 M LiTFSI/BMP TFSI at room temperature. 11 Moreover, the self-diffusivity of the mobile ions (Li+, BMP+, and TFSI-), lithium transference number (t_{Li^+}) , and conductivity were all found to be higher than the base ILE. The authors attributed the increase in ion mobilities to the enhanced ion pair dissociation as a result of the polyZI present. Interestingly, in contrast to the improved ion mobility results observed at room temperature, the poly(MPC) ionogel displayed a lower ionic conductivity than the base ILE at higher temperatures. Furthermore, the polyZI ionogel exhibited a lower activation energy of ionic conductivity (E_A) of 25.4 \pm 1 kJ/mol than the base liquid electrolyte with 29.2 \pm 1 kJ/mol. This decrease in E_A in the polyZI ionogel hinted at distinct mechanisms for ion transport in such materials.11

Although only a handful of published data exist to date on the zwitterionic-supported ionic liquid electrolytes, 4,11,18,19,22-24 the above findings suggest a promising approach to the development of electrolytes with high conductivity and elastic moduli. The research also indicates an existing knowledge gap of the competing electrostatic interactions in the polyZI-supported ionogels found between the zwitterion-charged groups, ionic liquids, and salt ions. Understanding such competing interactions will help open up a pathway for discovering new approaches for the design and improvement of next-generation ionogels. Additionally, a more complete understanding of these complex phenomena may allow for the decoupling of properties such as polymer dynamics and conductivity.

In this study, we use atomistic molecular dynamics simulations to investigate a model poly(MPC) supported LiTFSI salt-doped BMP TFSI ionogel. We pursued a systematic investigation focusing on the structure and dynamics of the ions to obtain a thorough understanding of the ion transport mechanisms that underlie the zwitterionic polymer-supported ionogels. Of specific interest was the ion transport mechanism of ${\rm Li}^+$ in the poly(MPC) ionogel and the difference, if any, relative to the base IL. Toward this objective, we varied the zwitterionic polymer content, lithium salt concentration, and temperature and probed the impact on the structure and dynamics of the poly(MPC) ionogel.

This paper is structured as follows—In Sec. II, we delineate the computational methods and setup. In Sec. III, we present the details of our methods of analysis. In Sec. IV, we present our results and discussion: In Sec. IV A, we discuss investigating the impact of varying polyZI content on the morphology (Sec. IV A 1) and the influence of varying salt concentration on morphology (Sec. IV A 2). In Sec. IV B, we present the influence of polymer content (Sec. IV B 1) and salt concentration (Sec. IV B 2) on ion dynamics. In Sec. IV C, we discuss the ion transport mechanisms. In Sec. V, we discuss the influence of temperature on the ion dynamics of the poly(MPC) ionogel and

compare it to the base ILE. Finally, we summarize our findings in Sec. $\ensuremath{\mathsf{VI}}$.

II. COMPUTATIONAL METHODS

In this work, we used atomistic molecular dynamic simulations to study polyZI-supported ionogel containing 2-methacryloyloxyethyl phosphorylcholine [poly(MPC)] in LiTFSI/BMP TFSI [poly(MPC) ionogel] (the chemical structures are displayed in Fig. 1). First, to understand the impact of polyZI content on the poly(MPC) ionogel, the number of BMP⁺, TFSI⁻, and Li⁺ ions was fixed and the number of poly(MPC) chains was varied (0–6 polyZI chains). The length of a single poly(MPC) chain was fixed to 15 monomer units. The polyZI content ($X_{\rm ZI}$) is expressed in terms of the ratio of the number of ZI units to the number of Li⁺ ions, as shown in Eq. (1). The simulation details for studying the impact of

varying $X_{\rm ZI}$ are shown in Table I. Second, to understand the impact of salt concentration on the poly(MPC) ionogel, the number of poly(MPC) chains was fixed (3 polyZI chains), and the salt content in the base ILE was varied. The salt content ($C_{\rm Li^+}$) is expressed as the ratio of the number of Li⁺ ions to the number of BMP⁺ ions, as shown in Eq. (2). The simulation details for understanding the impact of varying $C_{\rm Li^+}$ are shown below in Table II,

$$X_{\rm ZI} = \frac{n_{\rm ZI \ units}}{n_{\rm Li^+}},\tag{1}$$

$$C_{\rm Li^+} = \frac{n_{\rm Li^+}}{n_{\rm BMP}^+}.$$
 (2)

The molecular dynamics simulations were performed using the Gromacs 2020.5 package. ^{25,26} The all-atom optimized potential for liquid simulations (OPLS-AA) was used for modeling the

FIG. 1. Chemical structures for poly(MPC), BMP $^+$, and TFSI $^-$. X = 15 for the poly(MPC).

TABLE I. Simulation details for different poly(MPC) concentrations (XzI). The length of a single poly(MPC) polymer chain is fixed at 15.

System name	BMP^+	TFSI ⁻	Li ⁺	Poly(MPC) chains	MPC units	Box length (Å)	$C_{Li^+}(M)$	$X_{ m ZI}$	PolyZI weight (%)
$\overline{X_{\rm ZI}=0.0^{\rm a}}$	300	450	150	0	0	61.77	1.06	0.0	0.00
$X_{\rm ZI} = 0.1$	300	450	150	1	15	61.90	1.05	0.1	2.54
$X_{\rm ZI} = 0.2$	300	450	150	2	30	62.30	1.03	0.2	4.96
$X_{\rm ZI} = 0.3$	300	450	150	3	45	63.24	0.99	0.3	7.26
$X_{\rm ZI} = 0.4$	300	450	150	4	60	63.89	0.95	0.4	9.45
$X_{\rm ZI} = 0.5$	300	450	150	5	75	63.95	0.95	0.5	11.54
$X_{\rm ZI} = 0.6$	300	450	150	6	90	64.40	0.90	0.6	13.53

^aBase ILE for varying X_{ZI}.

TABLE II. Simulation details for different Li⁺ salt concentrations C_{1,i}⁺. The length of a single poly(MPC) polymer chain is fixed at 15.

System name	BMP ⁺	TFSI ⁻	Li ⁺	Poly(MPC) chains	MPC units	Box length (Å)	$C_{Li^+}(M)$	$X_{ m ZI}$	PolyZI weight (%)
$C_{\text{L},i^+} = 0.0^{\text{a}}$	300	300	0	3	45	59.13	0.00		9.49
$C_{\text{Li}^+} = 0.1$	300	330	30	3	45	59.91	0.23	1.50	8.94
$C_{\text{Li}^+} = 0.2$	300	360	60	3	45	60.53	0.45	0.75	8.45
$C_{\text{Li}^+} = 0.3$	300	390	90	3	45	61.68	0.64	0.50	8.01
$C_{\text{Li}^+} = 0.4$	300	420	120	3	45	62.47	0.82	0.38	7.62
$C_{\mathrm{Li}^+} = 0.5$	300	450	150	3	45	63.24	0.99	0.30	7.26

^aNo salt present.

poly(MPC) and the Li⁺ ion. ^{27,28} The CL & P force field²⁹ was chosen to model the BMP⁺-TFSI⁻-IL interactions. The total potential energy of the system in terms of its bonded and nonbonded potential interactions are displayed below in Eqs. (3) and (4), respectively,³⁰

$$U_b = \sum_b \frac{1}{2} k_b (b - b_0)^2 + \sum_\theta \frac{1}{2} k_\theta (\theta - \theta_0)^2 + \sum_\phi \sum_{m=1}^5 (-1)^m C_m (\cos \phi)^m + \sum_\psi \frac{1}{2} k_\psi (1 - \cos 2\psi).$$
 (3)

In Eq. (3), the bonded potential is modeled as the sum of the intermolecular bond, angle, dihedral, and improper torsions, where k_b , C_m , and k_θ denote bond length spring constants, bond angle spring constants, and Ryckaert–Bellemans potential constants, respectively. Furthermore, b are bond lengths, θ are bond angles, ϕ are the dihedral angles, and ψ is the improper dihedral angle. b_0 and θ_0 are the equilibrium bond lengths and angles, respectively,

$$U_{nb} = f_{ij} \left\{ \sum_{i < j} \frac{e^2 z_i z_j}{4\pi \varepsilon_0 r_{ij}} + 4\varepsilon_{ij} \left[\left(\frac{\sigma_{ij}}{r_{ij}} \right)^{12} - \frac{\sigma_{ij}}{r_{ij}} \right)^6 \right] \right\}. \tag{4}$$

Equation (4) displays the functional form of the nonbonded interactions, which are modeled as the sum of the electrostatic and Lennard–Jones (LJ) interactions scaled by f_{ij} , where $f_{ij} = 0$ for 1,2 and 1,3 interactions, $f_{ij} = 0.5$ for 1,4 interactions, and $f_{ij} = 1$ for interactions beyond 1-4 interactions. The geometric combining rule was used to generate the LJ parameters for cross terms.³⁰ The partial charges of the poly(MPC) were obtained by optimizing MPC trimers by applying B3LYP/6-311 g^{**} theory using Gaussian 16 Rev. C.01.³¹ The restrained electrostatic potential (RESP)³² was post-processed through the Multiwfn package. 33,34 The MPC repeating unit was constrained to net zero charge and averaged over two conformations of each trimer. The topology files of the poly(MPC) were obtained using MKTOP,³⁵ and in-house code was used to assemble the molecular structure and topology file. A factor of 0.8 was used to scale the atomic partial charges of the poly(MPC), lithium, and IL ions in the system to improve transport properties without implementing polarizable force fields. 16 The atom names associated with their GROMACS atom types and their corresponding LJ interaction parameters and atomic partial charges are listed in Tables S1-S4 in the supplementary material. The GROMACS atom types are associated with their corresponding bond angle, dihedral, and improper dihedral forcefield parameters in Tables S5–S13 in the supplementary material.

Inspired by the 21-step decompression method proposed by Colina and co-workers,³⁶ the following loop of the multistep equilibration procedure was used to prepare the equilibrated configuration:

- 1. 0.1 ns NVT (Canonical ensemble) simulation at 1000 K,
- 0.1 ns NPT (Isothermal-isobaric ensemble) simulation at 600 K and 100 bar, and
- 3. 0.1 ns NPT simulation at 600 K and 1 bar.

This three-step loop was repeated eight times in our study to prepare the initial configuration for the production run. A 110 ns NPT ensemble was employed for the production run. The initial 10 ns was used for equilibration, whereas the last 100 ns were used for analyzing the static and dynamic properties. The leapfrog integration scheme was used to integrate Newton's equations of motion.³⁷ A timestep of $\delta t = 1$ fs was used to update the simulations' force, velocity, and position. The Lennard–Jonnes (LJ) potential was set to 1.3 nm along with long-range electrostatic interactions calculated with the particle mesh method.³⁸ The v-rescale thermostat³⁹ was used for temperature coupling at 600 K with coupling parameters of τ_T = 1.0 ps. The Parrinello–Rahman barostat^{40,41} was used for pressure control at 1 bar with coupling parameters of τ_P = 1.0 ps. All simulations were run at 600 K to ensure that meaningful Li⁺ diffusivities were extracted. The average of five samples with different initial configurations was used to obtain the static and dynamic results presented in this work.

III. METHODS OF ANALYSIS

A. Radial distribution function

Ion-pair radial distribution functions, $g_{ij}(r)$, were calculated to describe the static interactions between species i and j in our poly(MPC) ionogel and the corresponding base ILEs,

$$g_{ij}(r) = \frac{V}{4\pi r^2 N_i N_j} \sum_i \sum_j \langle \delta(r - r_{ij}) \rangle.$$
 (5)

In the above, V is the volume of the simulation box, N_i and N_j are the number of molecules of species i and j, respectively, and δ is the Dirac delta function. The g(r) is used to define the

association distance, r_{ij}^* , which is utilized to determine the average number of molecules, j, coordinated within the first coordination shell of species i. The association distance cutoff (r_{ij}^*) is determined by the position r where the g(r) is minimum after the first peak. For poly(MPC), we chose the phosphorus atom in the phosphate group $[PO_4]$ and the nitrogen atom in the quaternary amine group $[N(CH_3)_3]$ to represent the anionic and cationic moieties in polyZI. For the BMP⁺, we use the nitrogen atom in the imidazolium to represent the IL cation, whereas for TFSI⁻, we use the nitrogen atom to represent the common anion. Finally, for the Li⁺ ion, we use the Li⁺ atom itself to obtain g(r)s.

B. Diffusion coefficients

The diffusion coefficients (D_i) were derived from the mean-squared displacements (MSDs) by using the Einstein relation,

$$D_{i} = \frac{1}{6} \lim_{t \to \infty} \frac{d}{dt} \langle [r_{i}(t+t_{0}) - r_{i}(t_{0})]^{2} \rangle, \tag{6}$$

where $r_i(t)$ is the position of the corresponding species i at time t. The representative atoms chosen are similar to those in the radial distribution function analysis. Due to the short time scale production of our simulations, we do not probe the diffusivity of poly(MPC) in our current study.

C. Ionic conductivity

The "ideal" ionic conductivity $(\sigma_{NE})^{42}$ was calculated using the following Nernst–Einstein equation:

$$\sigma_{NE} = \frac{q^2}{V k_B T} \sum_{i} N_i D_i, \tag{7}$$

where k_B is the Boltzmann constant, N_i is the number of corresponding molecules of species i, V is the system volume, and T is the temperature. The contribution of the poly(MPC) was neglected in the Nernst–Einstein conductivity.

D. Ideal transference number

The "ideal" lithium transference number^{43,44} was calculated based on the diffusion coefficients,

$$t_{\rm Li} = \frac{N_{\rm Li}D_{\rm Li}}{\sum_i N_i D_i},\tag{8}$$

where N_i is the number of corresponding molecules of species i and D_i is the diffusivity of corresponding molecules of species i. The contribution of the poly(MPC) was neglected in the ideal transference number.

IV. RESULTS AND DISCUSSION

A. Morphology

1. Influence of polyZI content on the morphology

We first discuss results for morphological characteristics of the poly(MPC) ionogel. In this section, we consider the case of varying polyZI content at a fixed salt concentration of 1 M LiTFSI/BMP TFSI. Figure 2 shows molecular dynamics (MD) simulation snapshots as a function of increasing polyZI content (X_{ZI}) (cf. Equation (1)). As the polyZI content is increased (left to right in the MD snapshots), we observe that Li⁺ and TFSI⁻ ions preferentially associate with the polyZI chains from the bulk Li salt doped ionic liquid (LiTFSI/BMP TFSI). At the higher polyZI content, we also observe an increasing association of BMP⁺ ions with the poly(MPC) chains lobserved through the gradual appearance of purple molecules (BMP+ ions) near the blue chains [poly(MPC)] with increasing $X_{\rm ZI}$]. This observation is further supported by the increasing BMP⁺-polyZI coordination observed with increasing X_{ZI} , as shown in Fig. S6(a). From these observations, we deduce that the anionic moieties (ZI[-]) of the polyZIs have a primary preference to associate with Li⁺ followed by a secondary preference to BMP⁺. With the increase in the polyZI content, we can see that the structural properties of the bulk ILE resemble more of a neat IL due to the increasing coordination of Li⁺ with the polyZIs. We also observe that the polyZI polymers are self-aggregated in Fig. 2. This polymer aggregation can also be seen clearly by removing Li⁺, TFSI⁻, and BMP+ ions from the MD snapshots, as shown in Fig. S2

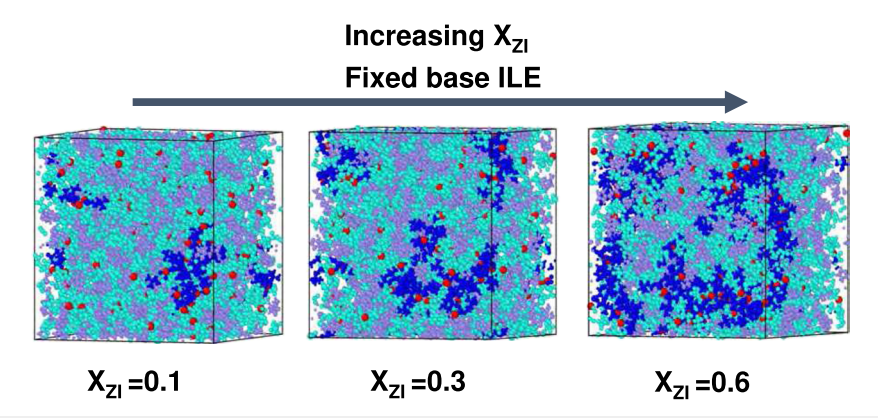


FIG. 2. Molecular Dynamics (MD) snapshots of simulation boxes with increasing X_{Zl} . Li⁺ (red), **TFSI**⁻ (teal), BMP⁺ (purple), and [poly(MPC) polymer] (blue) are displayed in the simulation snapshots.

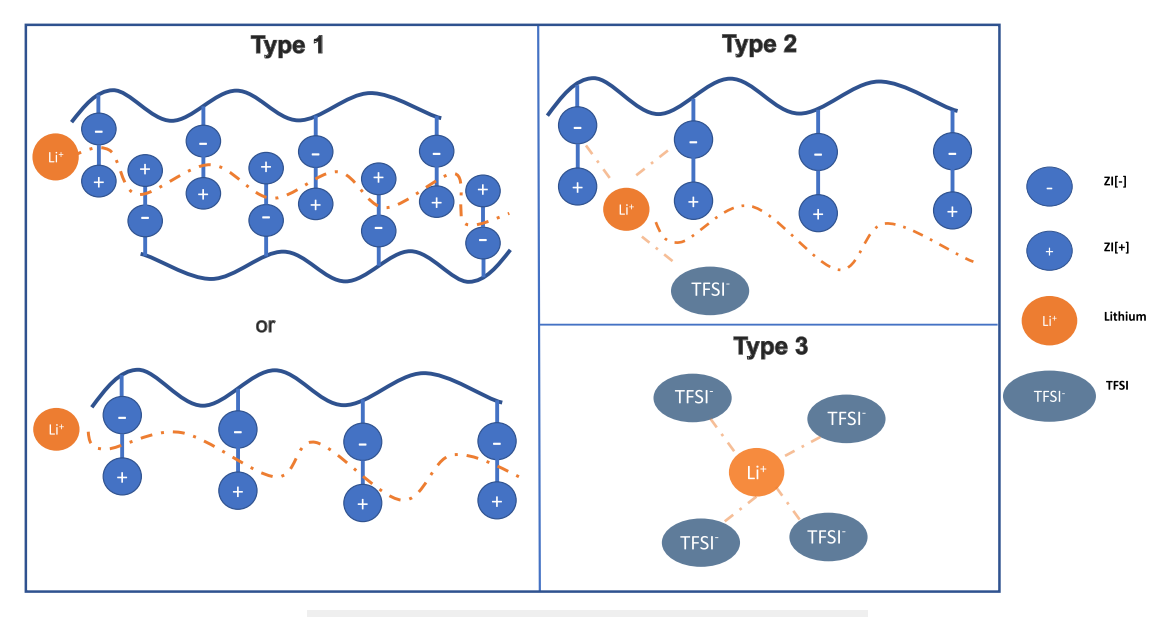


FIG. 3. Illustration of the different static coordination types of Li⁺ ions.

of the supplementary material. This is also further supported by the high intensity of ZI[-]-ZI[+] g(r) peaks in Fig. S4 (b) of the supplementary material. Overall, the observations suggest that the addition of polyZIs results in disruption in the interaction between Li⁺ and TFSI⁻ that exists within the bulk ILE. This aligns with the experimental results showing strong Coulombic interactions between Li⁺ and polyZI moieties, which disrupt the LiTFSI clusters found in the base ILE (LiTFSI/BMP TFSI).¹¹

To quantify the above observations on the influence of polyZI content, we follow our recent MD studies on salt-doped polymeric ionic liquids (PolyILs). ^{16,17} Therein, we pursued a systematic characterization of anion coordination in PolyILs based on its association with the anions and polycations by using the radial distribution function [g(r)] cutoff distances. ^{16,17} Similar to such a framework, in this present study, we categorized the Li⁺ ions in the poly(MPC) ionogel into three groups according to their coordination with the polyZI and TFSI⁻ by using the association distance of the first solvation shell of the g(r) (the g(r) results are discussed subsequently). In Fig. 3, we display a pictorial illustration of the classification of the different coordination types of Li⁺ ions presented in this work: type 1: Li⁺ exclusively coordinated with the polyZI chains, type 2: Li⁺ coordinated with both the polyZI chains and TFSI⁻, and type 3: Li⁺ exclusively coordinated with TFSI⁻.

Figure 4 shows the fractions of type 1, type 2, and type 3 Li⁺ present as a function of $X_{\rm ZI}$. At lower polymer content ($X_{\rm ZI}$), we observe that most of Li⁺ ions are present as type 3 and coordinated with TFSI⁻. With increasing $X_{\rm ZI}$, type 1 and type 2 Li⁺ coordinations are seen to increase, and correspondingly, the type 3 Li⁺ fraction decreases. Overall, with increasing $X_{\rm ZI}$, we observe an increase in Li⁺–ZI[-] associations accompanied with a decrease in exclusive Li⁺–TFSI⁻ interactions. These Li⁺ coordination trends confirm inferences drawn from Fig. 2 that Li⁺ ions preferentially associate with the polyZIs with increasing $X_{\rm ZI}$. Similar

characterization of BMP⁺ and TFSI⁻ coordination is presented in Secs. S4 and S5 of the supplementary material.

To understand the origins of the observed increased coordination of the mobile ions with the polyZI chains, we probed the radial distribution functions [g(r)] between different ion pairs. Figure 5 shows the g(r) results for (a) Li⁺ and ZI[-]([PO₄]⁻), (b) TFSI⁻ and ZI[+]([N(CH₃)₃]⁺), (c) Li⁺ and TFSI⁻, and (d) BMP⁺-TFSI⁻ as a function of $X_{\rm ZI}$. In Figs. 5(a) and 5(b), we observe that the g(r) between Li⁺-ZI[-] and TFSI⁻-ZI[+] do not change with increasing $X_{\rm ZI}$. This indicates that the Li⁺ and TFSI⁻ ions coordinated with the polyZI chains are subjected to the same interaction strength with the polymer regardless of the polymer content. However, in Fig. 5(c), as we increase $X_{\rm ZI}$ = 0.0 (no polyZI present) to $X_{\rm ZI}$ = 0.6, we see a reduction in the principal g(r) peak of Li⁺-TFSI⁻, which indicates

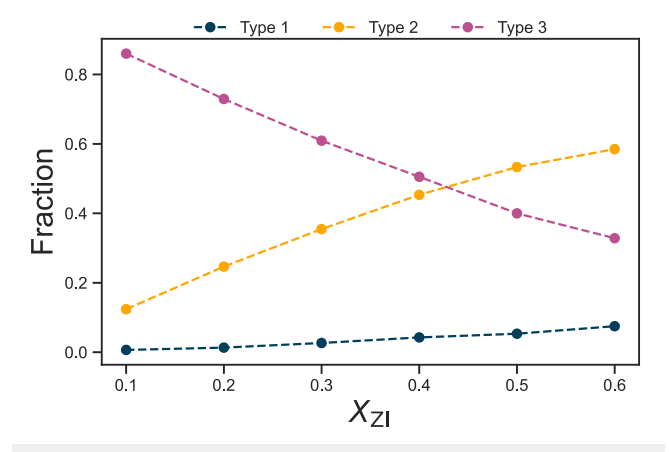


FIG. 4. Fraction of the different static coordination types of Li^+ as a function of X_{ZI} .

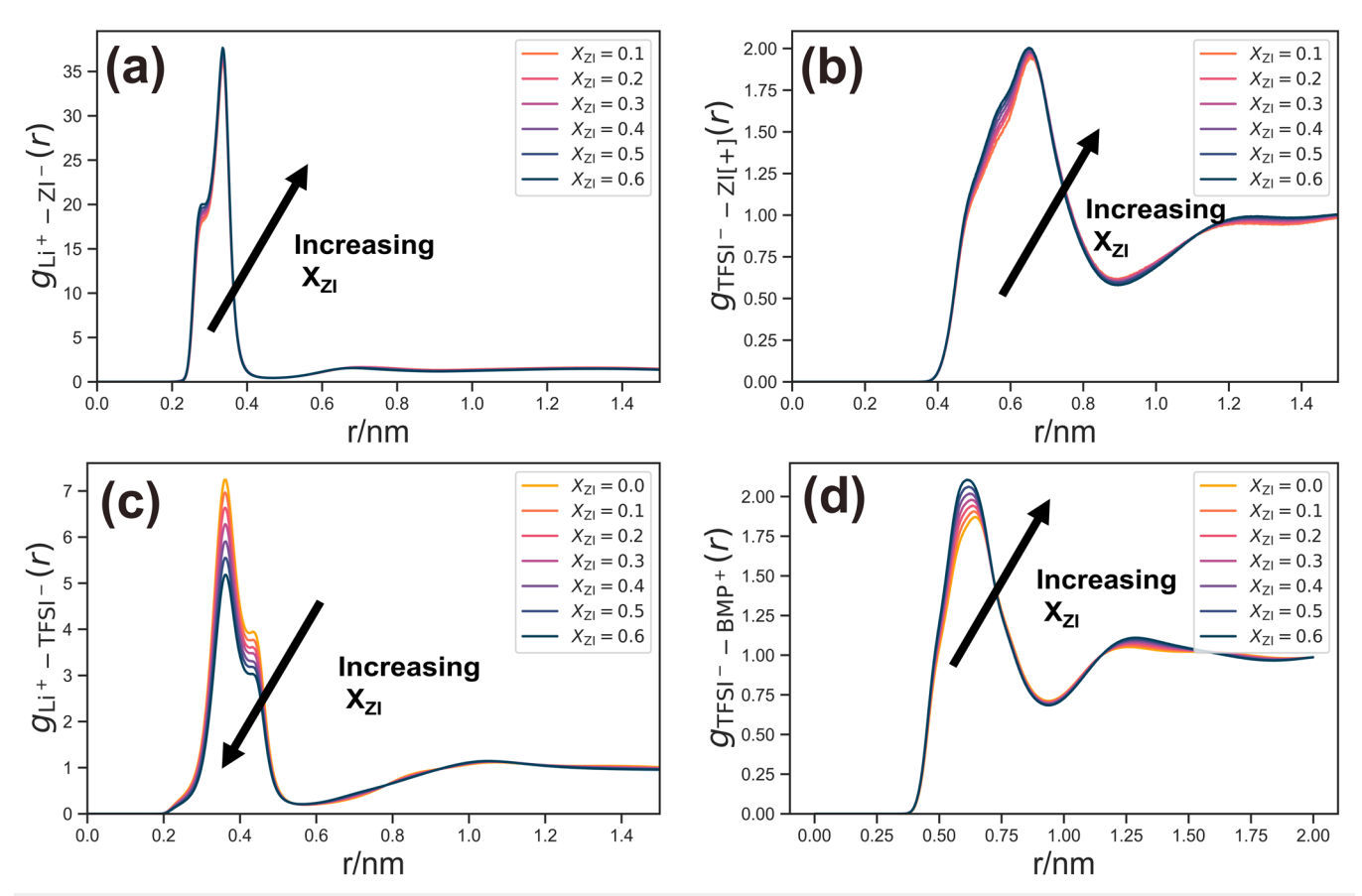


FIG. 5. Radial distribution functions for (a) Li⁺ and ZI[-]([PO_4]⁻), (b) TFSI⁻ and ZI[+]([$N(CH_3)_3$]⁺), (c) Li⁺ and TFSI⁻, and (d) BMP⁺-TFSI⁻ as a function of X_{ZI} in poly(MPC) supported 1 M LiTFSI salt-doped BMP TFSI ionogel systems. ZI[-] and ZI[+] represent the anionic and cationic moieties of the polyZI, respectively.

a reduction in the overall lithium–anion interaction with increasing $X_{\rm ZI}$. In contrast, in Fig. 5(d), the BMP⁺–TFSI⁻g(r) principal peak is seen to increase with increasing $X_{\rm ZI}$, indicating stronger interactions between the BMP⁺ and TFSI⁻ ion pairs with increasing $X_{\rm ZI}$. Such results again align with our morphology picture showing the

coordination of Li⁺ ions with the polyZIs results in the bulk IL structural properties of the system to resemble a neat IL as a result of the disrupted Li⁺-TFSI⁻ interactions. When reviewing the four interactions collectively in Fig. 5, it is evident that Li⁺ and ZI[-] exhibit interactions such that the peak in g(r) is almost 5 times

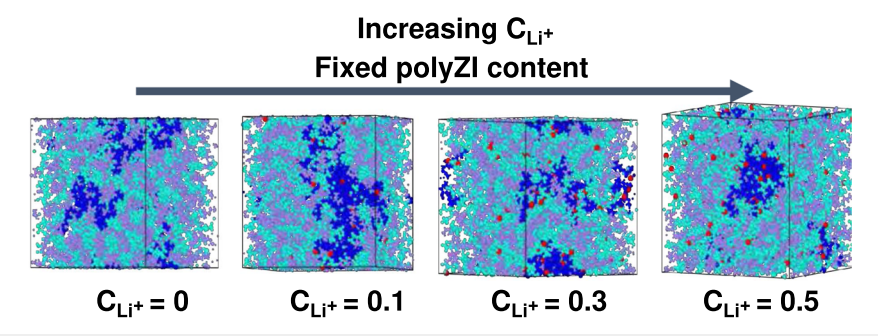


FIG. 6. Molecular Dynamics (MD) snapshots as a function of increasing C_{Li^+} . Li⁺ (red), **TFSI**⁻ (teal), BMP⁺ (purple), and [poly(MPC) polymers] (blue) are displayed in the simulation snapshots.

stronger than Li⁺ and TFSI⁻ and more than 15 times stronger than BMP⁺-TFSI⁻ and TFSI⁻-ZI[+] interactions. Such results serve to explain the origin of preferential coordination of Li⁺ ions with the polyZI chains. From the g(r) analysis, we can indeed conclude that the increased coordination of Li⁺ ions to the polyZI chains decreases the interaction between Li⁺ and TFSI⁻ and enhances the interaction between TFSI⁻ and BMP⁺.

2. Impact of varying salt concentration on the morphology

The results presented in this section relate to the protocol in which we varied the salt content (C_{L,i^+}) [cf. Eq. (2)] of a poly(MPC) ionogel at a fixed polyZI content equivalent to $X_{ZI} = 0.3$ (3 polyZI chains/45 ZI units). This system composition was selected due to the resemblance of its polymer weight content and salt concentration to the experimental setup. 11 Similar to the morphology analysis discussed in Subsection IV A 1, in Fig. 6, we present MD snapshots as a function of $C_{L,i}$ to provide a visual representation of the organization of the system. For $C_{\text{Li}^+} = 0$ (in the absence of LiTFSI salt), we can observe that the TFSI⁻ and BMP⁺ ions are associated with the polyZI chains. At $C_{I,i^+} = 0.1$, we see that the majority of the Li⁺ ions are associated with the polyZI chains. We also simultaneously observe a decrease in the association of BMP⁺ with the polyZI chains {observed through the gradual decrease of purple (BMP+) ions from the blue chains [poly(MPC)]}. This is due to the presence of Li⁺ and its preferential association with the poly(MPC). However, we do not observe a significant change in association of TFSI with the polyZI chains from the increased salt content ($C_{Li^+} = 0$ to $C_{\text{Li}^+} = 0.1$). For $C_{\text{Li}^+} > 0.1$, we observe an increasing fraction of Li⁺ and TFSI appearing in the bulk ionic liquid. For the concentration range of $C_{\rm Li^+}=0.1-0.5$, we do not observe a significant change in the association between BMP+ and TFSI-. This indicates that the increase in salt content does not substantially change the morphology of BMP⁺ and TFSI⁻ in the poly(MPC) ionogel. Similar to our observations in the context of varying polyZI content, we also observe polymer self-aggregation in Fig. 6. This is evident after the removal of Li⁺, TFSI⁻, and BMP⁺ ions from the MD snapshots, as shown in Fig. S3 of the supplementary material. This is also further supported by the high intensity of ZI[-]-ZI[+] g(r) peaks in Fig. S5(b) of the supplementary material.

To provide a more comprehensive quantitative description of the coordination change of Li⁺ ion with respect to the polyZI chains and TFSI $^-$ as a function of C_{Li^+} , we again present the fraction of the different coordination types of Li⁺ in Fig. 7. The coordination statistics of TFSI⁻ and BMP⁺ are presented in Secs. S4 and S5 of the supplementary material. At the lowest salt concentration, C_{Li^+} = 0.1, the system is seen to be mainly comprised of 35% type 1 and 60% type 2 Li⁺. These statistics suggest that almost 95% of the Li⁺ are coordinated with the polyZI chains, indicating that almost all the Li⁺ are associated with the polyZIs. This closely aligns with the physical picture in the MD snapshots shown in Fig. 6, indicating the preferential association of Li⁺ ions to the polyZI chains. As the salt concentration is increased to $C_{Li^+} = 0.2$, we observe a slight increase in type 2 Li⁺, a significant decrease in type 1 Li⁺, and an increase in type 3 Li⁺ fractions. Such results are consistent with the MD snapshots, which show an increase in Li⁺-TFSI⁻ associations and a decrease in Li^+ -polyZI associations with increasing C_{Li^+} . For the concentration range $C_{Li^+} > 0.2$, the type 1 and type 2 Li⁺

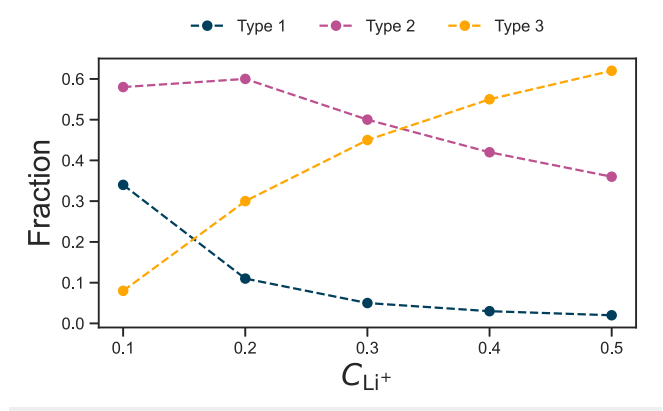


FIG. 7. Fraction of the different static coordination types of Li⁺ as a function of C_{Li^+} .

fractions monotonically decrease, while the type 3 Li⁺ fraction increases. Type 1 Li⁺ is seen to become negligible for $C_{\text{Li}^+} > 0.3$. Overall, we observe that in the lower salt concentration ranges $C_{\text{Li}^+} < 0.3$, type 1 and type 2 Li⁺ dominate the ion coordination statistics. Meanwhile, in the higher concentration region, we observe that type 3 Li⁺ dominates the ion-coordination statistics. This is consistent with the physical picture of the MD simulation snapshots, showing that the majority of Li⁺ ions are present in the bulk ILE at higher salt concentrations. Furthermore, we can conclude that the addition of LiTFSI salt changes the bulk ILE structural properties to resemble the structure of LiTFSI salt-doped BMP TFSI. Based on the results, we can infer that the addition of salt in a polyZI ionogel leads to a behavior qualitatively opposite to that observed while increasing the polymer content (Sec. IV A 1).

Next, we probed the radial distribution functions, g(r), to understand the structural characteristics arising from changing C_{Li} . Figure 8 shows g(r) for (a) $Li^+-ZI[-]$, (b) $TFSI^--ZI[+]$, (c) $Li^+-ZI[-]$ TFSI⁻, and (d) BMP^+ -TFSI⁻ as a function of C_{Li^+} . The principal g(r) intensity strength shows the interaction strength in the order of $Li^+-ZI[-] \gg Li^+-TFSI^- > BMP^+-TFSI^--TFSI^--ZI[+]$. This trend is similar to the g(r) trends observed in Fig. 5 while studying the impact of varying polyZI content. It is also evident in Figs. 8(a) and 8(d) that we observe a decrease in the intensity of interaction between Li^+ –ZI[-] and BMP^+ – $TFSI^-$ with increasing C_{Li^+} . We attribute this to the decreased coordination of Li⁺ ions with the polyZIs, which could disrupt the BMP⁺-TFSI⁻ associations present in the neat IL. In Fig. 5(b), we observe that the interaction strength between TFSI $^-$ -ZI[+] is not affected as a function of C_{Li^+} . This is due to the consistent TFSI--ZI[+] association observed in the MD snapshots at all salt concentrations, C_{Li} . In contrast, in Fig. 8(c), we observe an increasing interaction between Li⁺-TFSI⁻ with increasing salt content. With increasing $C_{L,i}$, we also note the observed trends in Figs. 8(c) Li⁺-TFSI⁻ and Figs. 8(d) BMP⁺-TFSI⁻ are opposite to the trends observed when increasing X_{ZI} , as shown in Fig. 5.

Overall, from the MD snapshots, ion-coordination statistics, and g(r) analyses, we can derive a comprehensive understanding of the influence of salt concentration and polymer content on the structural properties. First, we deduce a strong preference of Li⁺ ions to coordinate with the polyZIs. Second, we can surmise that an

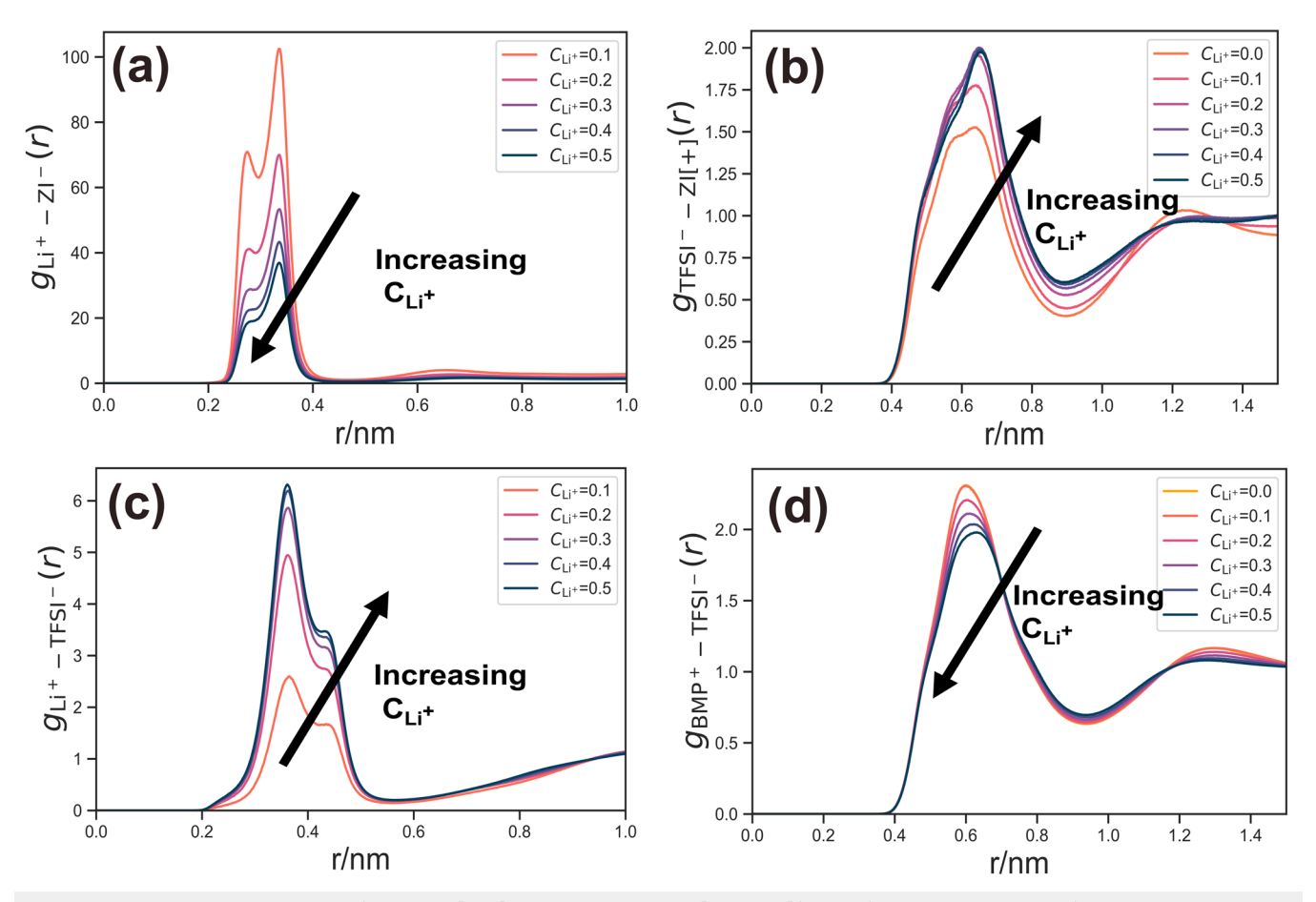


FIG. 8. Radial distribution functions for (a) Li⁺ and ZI[-]([PO₄] $^-$), (b) TFSI $^-$ and ZI[+]([N(CH₃)₃] $^+$), (c) Li⁺ and TFSI $^-$, and (d) BMP⁺–TFSI $^-$ as a function of salt concentration (C_{Li^+}). ZI[-] and ZI[+] represent the anionic and cationic moieties of the polyZI, respectively.

increase in salt concentration brings the bulk IL structural properties of the system closer to a lithium salt-doped ionic liquid, whereas an increase in the polyZI content brings the bulk IL structural environment close to a neat IL (ionic liquid with no salt present).

B. Ion dynamics

1. Influence of polyZI content on the ion dynamics

In this section, we present the results for the influence of polymer content on ion dynamics. In Fig. 9, we present diffusivities of the mobile ion species as a function of $X_{\rm ZI}$. We observe that the mobility of all ion species monotonically decreases with increasing $X_{\rm ZI}$. Broadly, this can be understood as arising from the increased coordination of the Li⁺, BMP⁺, and TFSI⁻ ions with the immobile polyZI chains with increasing $X_{\rm ZI}$, as shown in the MD snapshots in Fig. 2. Consistent with the morphology results, we also observe a more pronounced decrease in the Li⁺ diffusivity. This may be attributed to the strong Li⁺–ZI[-] interactions observed along with the preferential coordination of Li⁺ ions with the polyZIs.

To further understand the origins of the Li^+ ion dynamics of the poly(MPC) ionogel as a function of X_{ZI} , we drew inspiration

from our previous MD study on salt-doped PolyILs to probe the short-time mean square displacements of type 1, type 2, and type 3 $\rm Li^+$ ions. 16,17 Figure 10 displays the short-time mean squared displacements of (a) total $\rm Li^+$ ions, (b) type 1, (c) type 2, and (d) type 3

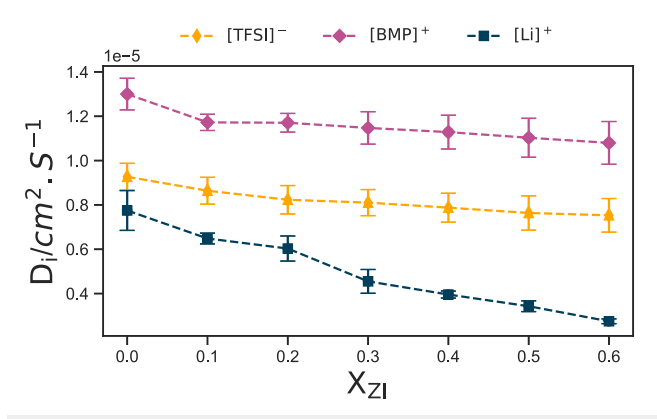
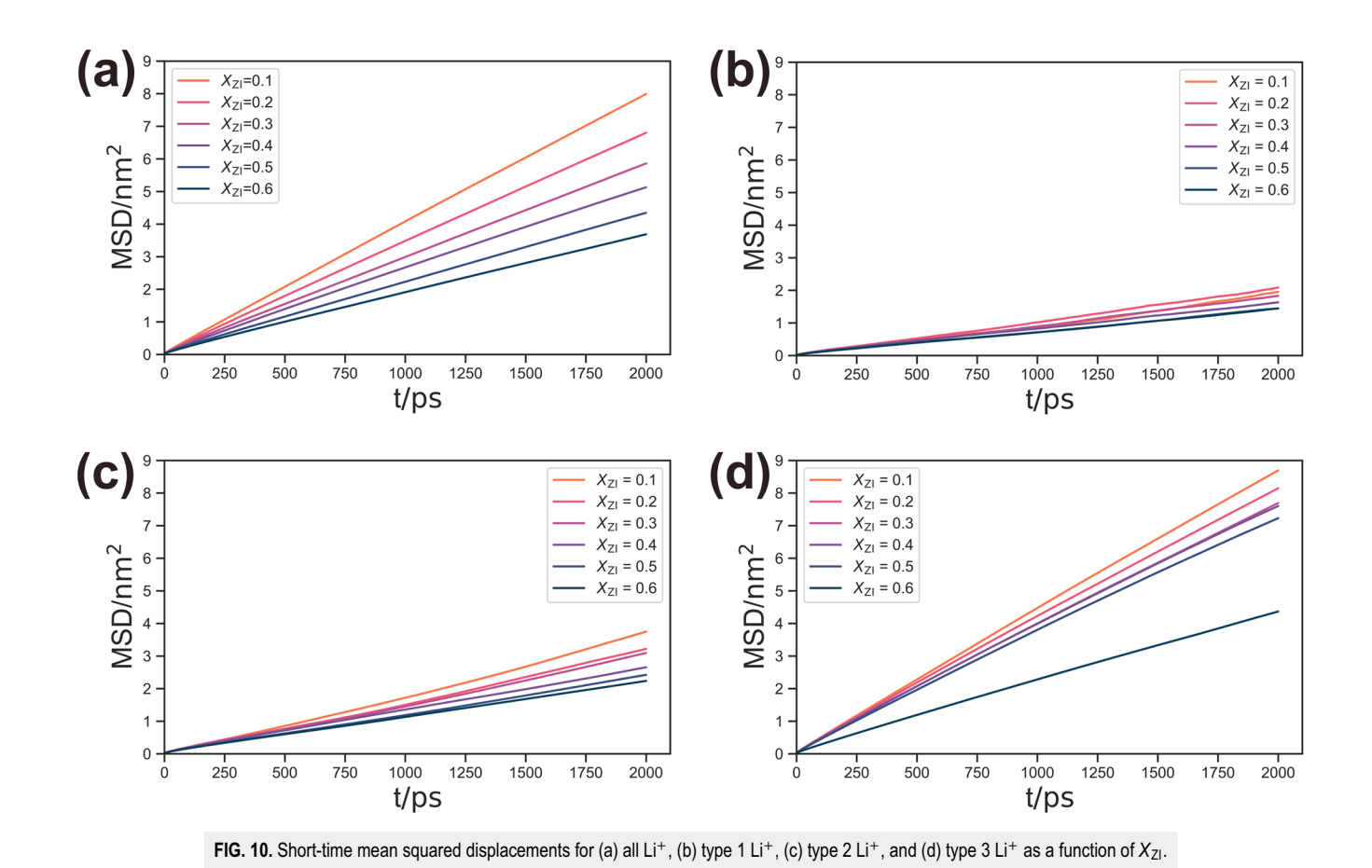


FIG. 9. Self-diffusion coefficient as a function of zwitterion polymer content $(X_{Z|})$.



Li⁺ ions. In Fig. 10(a), consistent with the Li⁺ diffusivity results, we observe that the total Li⁺ short-time MSD decreases with increasing $X_{\rm ZI}$. In Figs. 10(b)–(d), we also observe the short-time MSD of type 1, type 2, and type 3 Li⁺ ions decreasing with increasing $X_{\rm ZI}$.

Furthermore, the results show the order of their dynamics as follows: type $3 \text{ Li}^+ \gg \text{type } 2 \text{ Li}^+ > \text{type } 1 \text{ Li}^+$. This indicates that the dynamics of the Li⁺ ions associated exclusively with the anions display faster dynamics than the Li⁺ ions associated with poly(MPC).

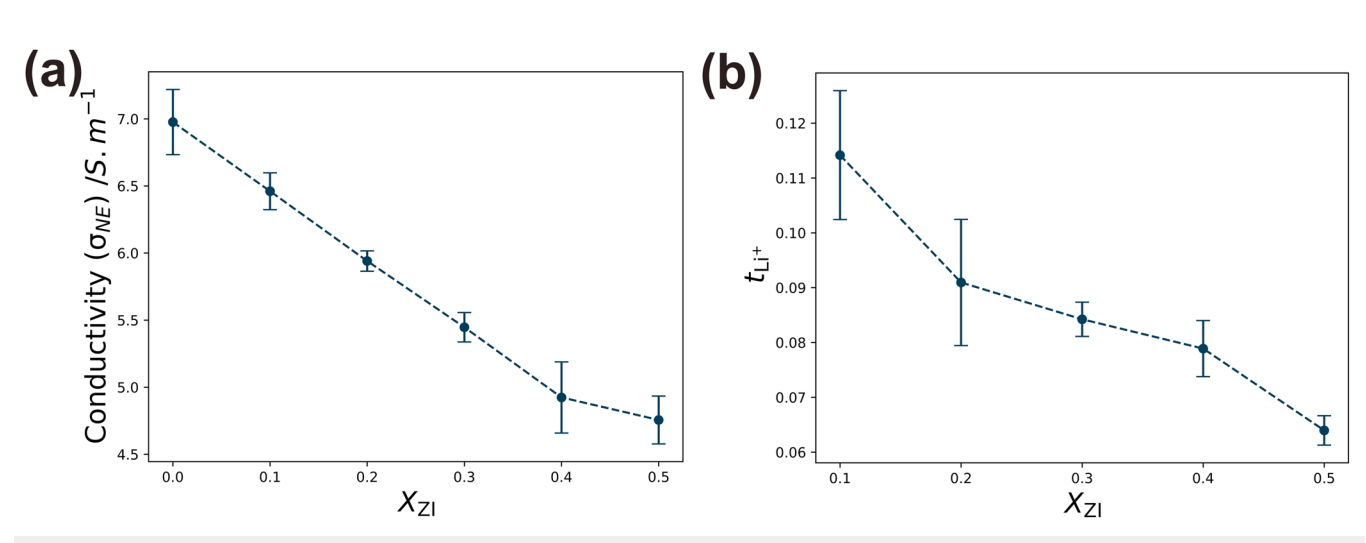


FIG. 11. (a) Nernst–Einstein conductivity and (b) "ideal" transference numbers as a function of X_{ZI} for poly(MPC)-supported LiTFSI/BMP TFSI and the base ILE- LiTFSI/BMP TFSI

This is due to the relatively strong Li⁺–ZI[–] interactions, as shown in the g(r) results of Fig. 5(a). Furthermore, we can interpret the overall dynamics of Li⁺ as a result of a compensation effect between the faster dynamics of type 3 Li⁺ ions and the slower dynamics of type 2 and type 1 Li⁺ ions. Therefore, the decreasing Li⁺ diffusivity observed with increasing $X_{\rm ZI}$ can be understood as arising from the increasing coordination of Li⁺ with the polyZI (increasing type 1 and type 2 Li⁺ ions) with increasing $X_{\rm ZI}$, as shown in Fig. 4.

To quantify the impact of $X_{\rm ZI}$ on the dynamics of the poly(MPC) ionogel relative to that of the base ILE, we calculated the Nernst–Einstein conductivity ($\sigma_{\rm NE}$) and the ideal lithium transference number ($t_{\rm Li^+}$) using Eqs. (7) and (8), respectively. The corresponding results are displayed in Fig. 11. In Fig. 11(a), we observe that the base ILE ($X_{\rm ZI}$ = 0) displays the highest conductivity followed by a decrease in the conductivity with increasing $X_{\rm ZI}$. In Fig. 11(b), we also observe a decreasing lithium transference number with increasing $X_{\rm ZI}$. Overall, the decrease in conductivity and lithium transference number can be attributed to the increased coordination of the mobile ions with the immobile poly(MPC) chains with increasing $X_{\rm ZI}$, as shown in MD snapshots and coordination statistics in Sec. IV A 1.

2. Impact of varying salt concentration on ion dynamics

Next, to understand the influence of salt concentration on the dynamics of the mobile ion species, we present the diffusivities in poly(MPC) ionogel and compare them with the base ionic liquid (base ILE)-Li TFSI/BMP TFSI as a function of C_{Li^+} in Figs. 12(a) and 12(b). In Fig. 12, our findings indicate that the diffusion coefficients of the mobile ion species in the poly(MPC) ionogel are slower than the monomeric base ILE. This is consistent with the experimental findings at temperatures higher than 300 K. ¹¹ In Fig. 12(a), for the poly(MPC) ionogel, we observe an increasing trend in the Li⁺ diffusion coefficient with increasing salt concentration from $C_{\text{Li}^+} = 0.1 - 0.5$. For the TFSI⁻ and BMP⁺ ions, we observe a slight decrease in mobility with increasing C_{Li^+} . In comparison to the

Li⁺ mobility, the TFSI⁻ and BMP⁺ mobilities are found to be less sensitive to the salt concentration.

In contrast to the poly(MPC) results, in the base ILE [Fig. 12(b)], we observe a decrease in the mobility of all ions with increasing $C_{\rm Li^+}$. Such diffusivity trends have been commonly observed in salt-doped ILEs and have generally been attributed to the increase in viscosity resulting from the additional salt content in the already ion-dense ionic liquid environment.⁴⁵

To understand the differences in Li⁺ diffusivity trends between the poly(MPC) ionogel and base ILE, we probed the short-time mean square displacements of type 1, type 2, and type 3 Li⁺ ions. In the results displayed in Fig. 13(a), we observe that the total Li⁺ shorttime mean square displacements increase with an increasing $C_{i,i}$ in agreement with the D_{Li^+} displayed in Fig. 12(a). In Figs. 13(b) and 13(c), we also observe that the mobilities of type 1 and type 2 Li⁺ increase with increasing C_{Li^+} , respectively. This can be attributed to the decreasing interaction strength observed in Li^+ –ZI[-] g(r)with increasing C_{Li^+} (Fig. 8). In Fig. 13, for type 3 Li⁺, we observe that the mobility becomes slower with increasing C_{Li^+} . The latter trends are similar to the behavior exhibited by Li+ in salt-doped monomeric ILs, as shown in Fig. 12(b). Moreover, type 3 Li⁺ is seen to be faster than the dynamics of type 1 and type 2 Li⁺ ions. Similar to Sec. IV B 1, the slower dynamics of type 1 and type 2 Li⁺ can be attributed to their coordination with the immobile polyZI matrix, while the faster dynamics of type 3 Li+ can be attributed to the presence of bulk ILE. Furthermore, we observe that the net Li⁺ mobility in the poly(MPC) ionogel represents a compensation between the decreasing mobility of Li⁺ associated with the anion exclusively (type 3) and the increasing mobility of Li⁺ associated with polyZI and/or TFSI- (type 1 and type 2 Li+) with increasing C_{Li}+. In other words, the net Li⁺ diffusivity increases due to the increasing type 3 Li⁺ fraction and decreasing type 1 and type 2 Li⁺ ion fractions with increasing C_{Li^+} observed in Fig. 7.

To further compare and contrast the impact of C_{Li^+} on the dynamics of the poly(MPC) ionogel relative to that of the base ILE, we calculated the Nernst–Einstein conductivity (σ_{NE}) and the ideal

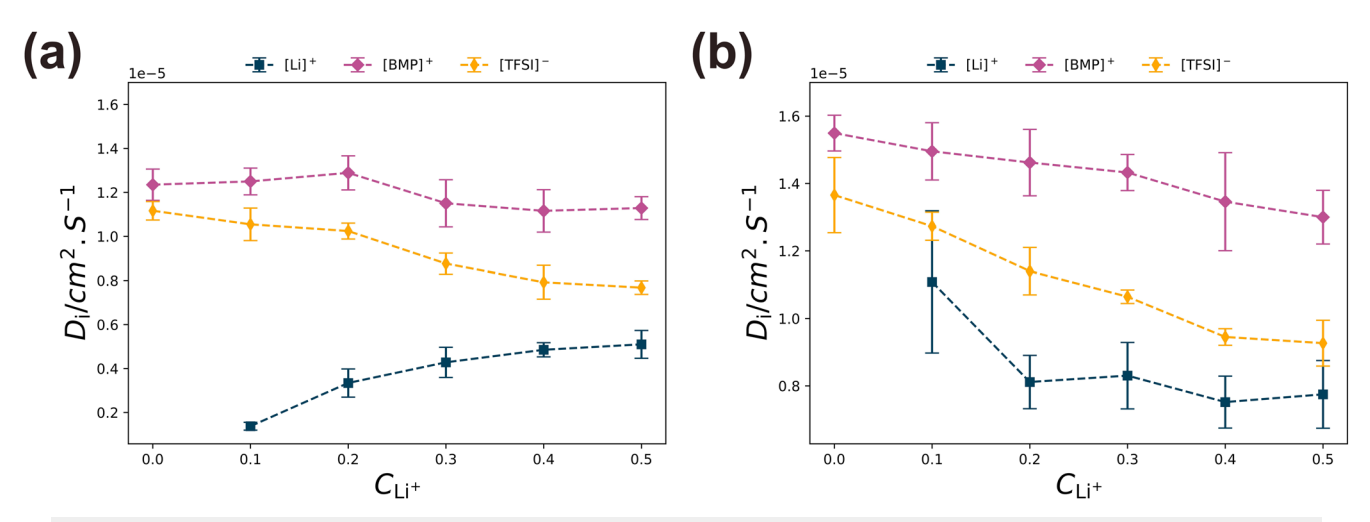
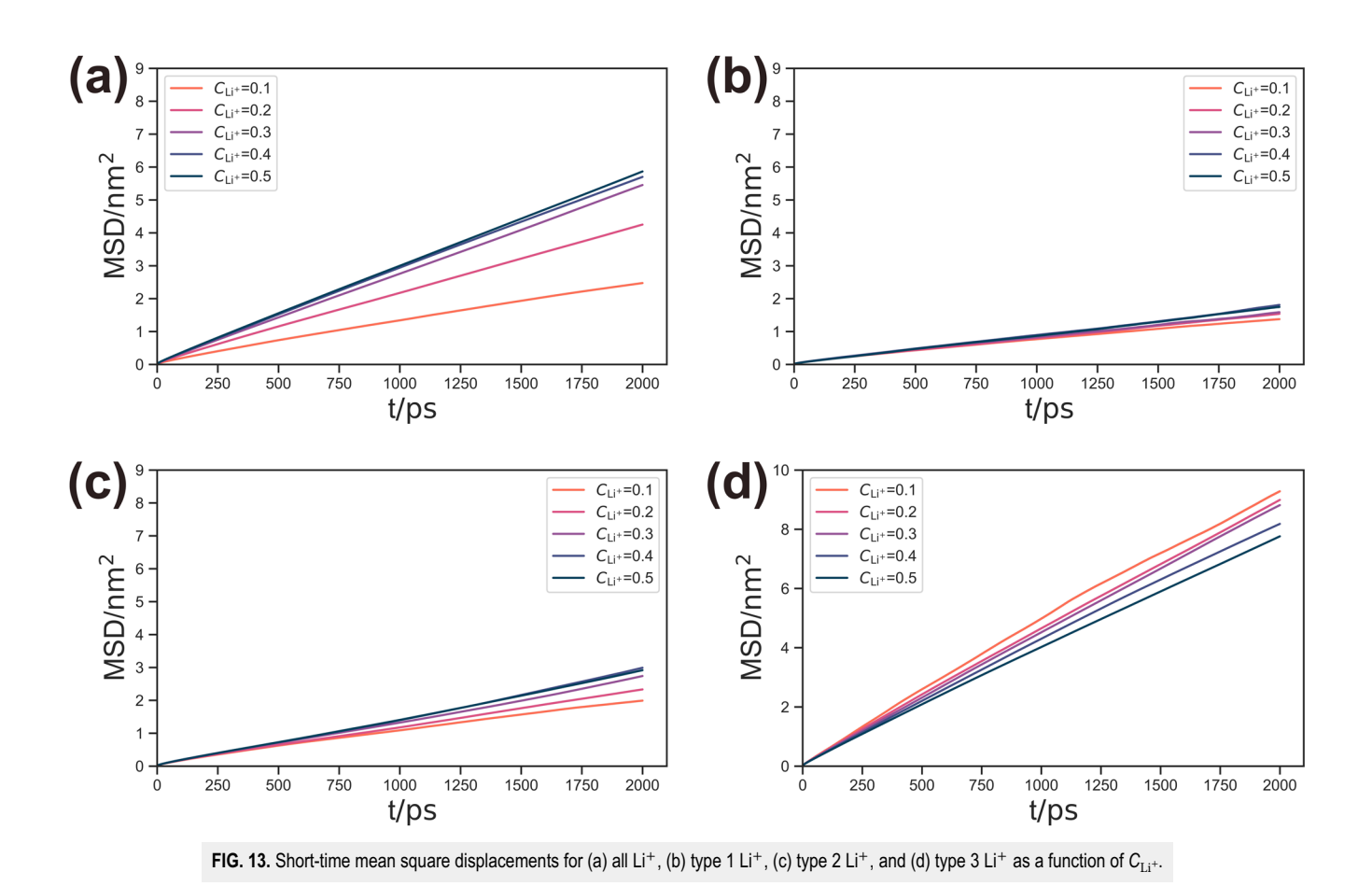


FIG. 12. Diffusion coefficients of Li⁺, TFSI⁻, and BMP⁺ as a function of salt concentration $C_{1,i}$ for (a) poly(MPC) ionogel and (b) base ILE (LiTFSI in BMP TFSI).



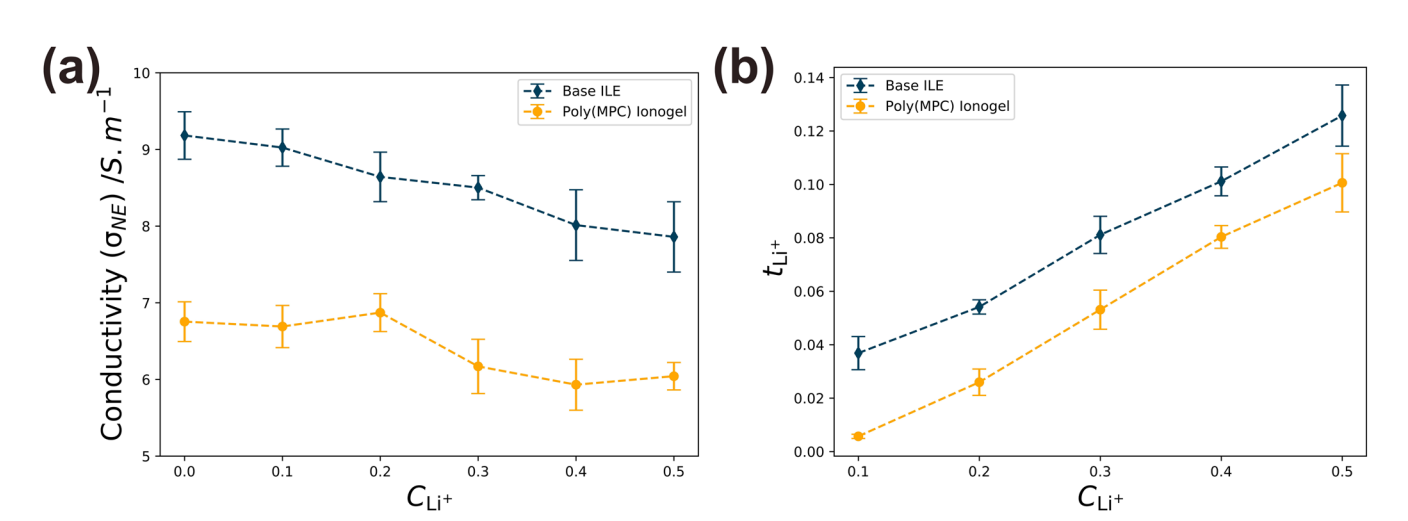


FIG. 14. (a) Nernst–Einstein conductivity and (b) "ideal" transference numbers as a function of $C_{\mathrm{Li^{+}}}$ for poly(MPC)-supported LiTFSI/BMP TFSI and the base ILE-LiTFSI/BMP TFSI.

transference number ($t_{\rm Li^+}$) using Eqs. (7) and (8), respectively. In Fig. 14, we observe that both the magnitude of conductivity and ideal transference number of the poly(MPC) ionogel are lower than the base ILE. This trend is in accordance with the experimental results for 1 M LiTFSI/BMP TFSI and poly(MPC) supported 1 M LiTFSI/BMP TFSI ILE [poly(MPC) ionogel] at T > 300 K.¹¹ Furthermore, Fig. 14(a) shows the that Nernst–Einstein conductivity is nearly constant as a function of $C_{\rm Li^+}$ for both the poly(MPC) ionogel and the base ILE. In Fig. 14(b), we observe that the ideal transference number increases with increasing $C_{\rm Li^+}$ for the poly(MPC) ionogel and the base ILE.

In conclusion, for the poly(MPC) ionogel, we observe a decreasing BMP⁺ and TFSI⁻ diffusivity trend as a function of both $X_{\rm ZI}$ and $C_{\rm Li^+}$. The trend of the Li⁺ diffusivity of the poly(MPC) ionogel contrasted with the base ILE as a function of $C_{\rm Li^+}$. This was attributed to the compensation of the dynamics of Li⁺ associated exclusively with TFSI⁻ and Li⁺ associated with the poly(MPC). The conductivity and ideal lithium transference number of the poly(MPC) ionogel were found to be lower than their respective base ILEs as a function of both $X_{\rm ZI}$ and $C_{\rm Li^+}$ for these simulations conducted at a temperature of 600 K. These conductivity and lithium transference number results align qualitatively with the experimental data. ¹¹

C. Ion transport mechanisms

In the introduction (Sec. I), we highlighted that one of the experimental observations of Panzer and co-workers related to the

poly(MPC) ionogel exhibiting a lower apparent activation energy of ionic conductivity (E_A) compared to its base ILE containing 1 M LiTFSI/BMP TFSI. ^{11,18,19} Such a result was hypothesized to arise from a change in the ion transport mechanisms with the introduction of the polyZI. 11,18,19 For a Li⁺ salt-doped polymer-supported electrolyte, commonly three types of Li⁺ ion transport mechanisms are discussed in the literature: vehicular diffusion, structural diffusion, and hopping mechanism. 23,44,46 The vehicular diffusion mechanism, as implied in the name, is a mode of transport in which the Li⁺ ion moves in a coupled manner with the anions in its solvation shell. In structural diffusion, Li⁺ ion moves by forming and breaking coordination with the anions in its first solvation shell. The hopping mechanism refers to the motion of Li⁺ via "hopping" between different sites along the polymer backbone. For Li salt-doped ILs, MD simulations have shown the importance of the vehicular transport mechanism for Li⁺ ion transport at low salt concentration, with the importance of structural diffusion increasing with salt content. 45

In Fig. 15, we present an illustration of the criteria we used to analyze the Li⁺ ion transport mechanisms. For Li⁺ ions associated with the anions (types 2 and 3), we considered whether they travel via a vehicular or structural diffusion mechanism. To distinguish such modes, the travel length of Li⁺ before the first solvation shell is refreshed is used as the criterion. For our analysis, we consider a solvation shell to be intact (not refreshed) if it retains at least one of its anions. If the Li⁺ ion travels less distance than twice the radius of gyration (*Rg*) of the solvating molecule before the solvation shell refreshes, then it is considered a structural diffusion. ¹⁶ However, if the Li⁺ within its solvation shell travels a distance greater than 2*Rg*

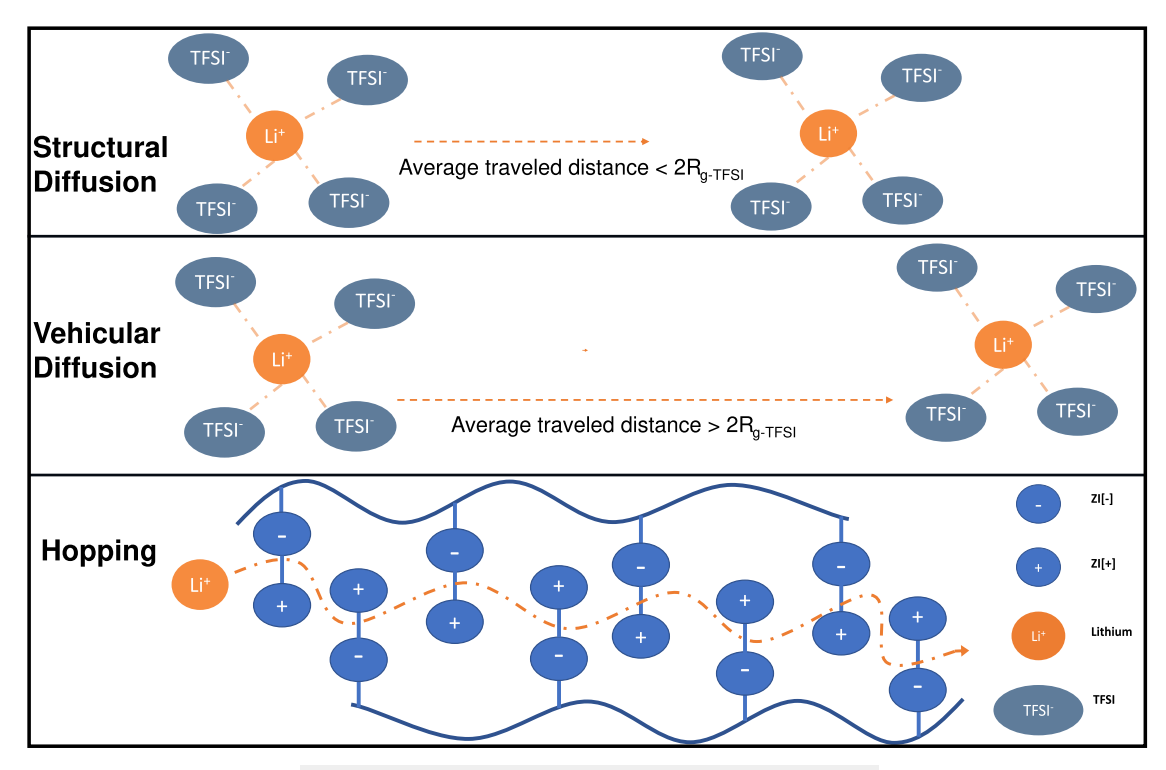


FIG. 15. Illustrations of the three types of Li⁺ ion transport mechanisms.

of the solvating molecule without the solvation shell refreshing, then it is considered a vehicular transport mechanism. ¹⁶ Finally, for the type 1 Li⁺ ions exclusively coordinated with the polyZIs, we hypothesize that they move within the polymer matrix through a "hopping" like mechanism. The presence of a hopping mechanism in type 1 Li⁺ ions is probed by examining the coordination of individual Li⁺ ions with the polymer chains as a function of simulation time. In this section, first, we present the findings of the ion transport mechanism of the Li⁺ ions coordinated with the anions (types 2 and 3 Li⁺), followed by the ion transport mechanism of the Li⁺ ions exclusively coordinated with the polymer (type 1 Li⁺).

1. Ion transport mechanisms for type 2 and type 3 Li⁺ ions

To investigate the ion transport mechanism of Li⁺ associated with TFSI-, we calculated the average travel length of type 2 and type 3 Li⁺ ions before its solvation shell is refreshed. The corresponding results are displayed in Fig. 16(a) as a function of X_{ZI} . The dashed line in Fig. 16(a) shows twice the radius of gyration of TFSI⁻ $(2R_{g-TFSI})$ used to distinguish between structural and vehicular ion transport mechanisms. As X_{ZI} increases, we can see that the average travel length of the Li+ solvation shell decreases, indicating a decrease in vehicular transport and an increase in structural diffusion. For X_{ZI} < 0.3, the ionogel shows an average travel length higher than $2R_{\rm g-TFSI}$, which indicates a dominant vehicular transport mechanism. We recall that in the lower poly(MPC) content ionogels ($X_{ZI} < 0.3$), the majority of Li⁺ ions have type 3 Li⁺ coordination status. From this, we can infer that type 3 Li⁺ travels via a vehicular transport mechanism. For $X_{ZI} = 0.6$, we observe that the average travel length of the Li⁺ is slightly lower than twice the radius of gyration (2Rg), which indicates the increased existence of structural diffusion. We recall from Fig. 4 that at $X_{ZI} = 0.6$, the majority of the Li⁺ associated with the anions are type 2 Li⁺. Therefore, this analysis suggests that type 2 Li⁺ ions travel via a structural diffusion mechanism.

To quantify the relative quantitative magnitude of the Li⁺ ion transport mechanisms for type 2 and type 3 Li⁺ ions, we calculated the fraction of vehicular and structural diffusion mechanisms present as a function of $X_{\rm ZI}$. As per the criteria specified above, a travel length distance of twice the radius of gyration of TFSI⁻ was used to distinguish whether Li⁺ associated with anions traveled via vehicular or structural diffusion. Figure 16(b) shows the fraction of the structural and vehicular transport mechanism present for Li⁺ associated with the anions (types 2 and 3) as a function of $X_{\rm ZI}$. We observe an increasing structural transport mechanism with an increase in $X_{\rm ZI}$, which further supports the average Li⁺ solvation shell travel length analysis. This indicates that the addition of poly(MPC) may cause frequent refreshing of the Li⁺ solvation shell resulting in an increased structural diffusion in the poly(MPC) ionogels.

2. Ion transport mechanisms for type 1 Li⁺ ions

Next, we probe the presence of a hopping mechanism in type 1 Li⁺ ions by concurrently investigating the dynamic and static properties of *individual* Li⁺ ions as a function of time. Figure 17 displays a sample of the analysis showcasing (a) mean squared displacement, (b) Li⁺–poly(MPC) chain coordination statistics, and (c) Li⁺–TFSI⁻ coordination of an individual Li⁺ ion at C_{Li^+} = 0.1. In Figs. 12(b) and 12(c), the y-axis represents the 45 ZI chain units present and the 450 TFSI⁻ molecules present in the system. The solid and dashed lines indicate the coordination of Li⁺ to the respective molecules. The presence of multiple lines at a particular time frame suggests the coordination of Li⁺ with multiple species at that time frame.

In Figs. 17(b) and 17(c), the sample Li⁺ ion is seen to change its coordination status with the polyZI and TFSI⁻ throughout the entire trajectory. We can observe the Li⁺ coordination status (types 1, 2, and 3) changing as indicated by the labels in Fig. 17. Type 1 Li⁺ coordination characterized by the coordination with the polyZI chains and the absence of coordination with TFSI⁻ shows relatively minor MSD fluctuations. Here, we observe some association, dissociation, and re-association of type 1 Li⁺ with neighboring polyZI

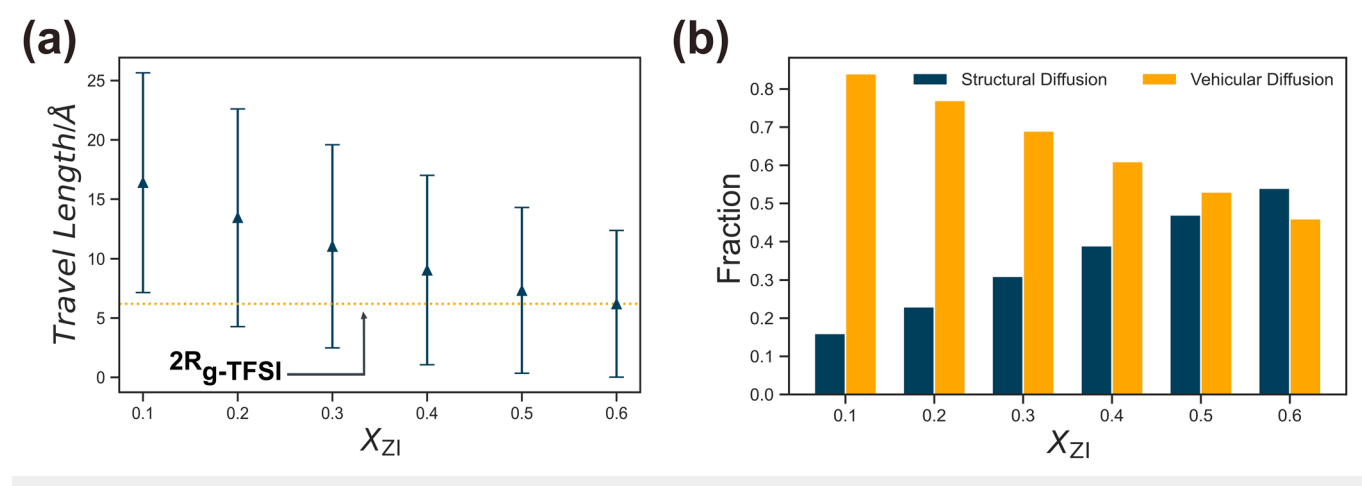


FIG. 16. (a) Average travel length of the Li⁺ solvation shell before the first solvation shell dies and (b) the fraction of structural and vehicular transport mechanism for types 2 and 3 as a function of X_{Zl} .

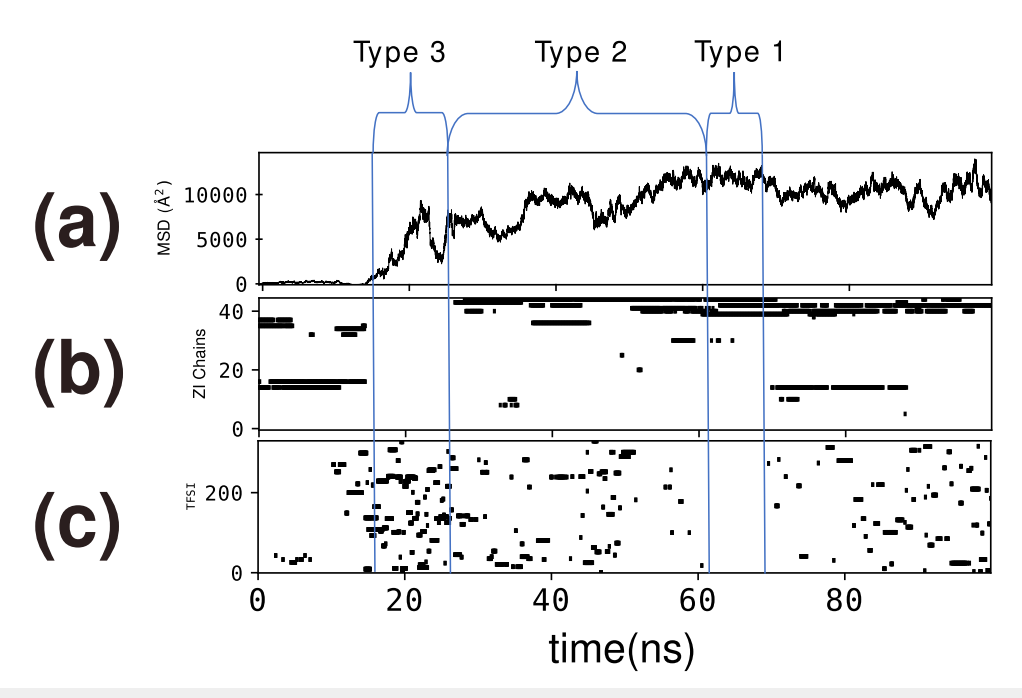


FIG. 17. Concurrent analysis showcasing (a) mean squared displacement, (b) Li^+ -poly(MPC) chain coordination statistics, and (c) Li^+ -TFSI $^-$ coordination of an individual sample Li^+ ion at $C_{Li^+} = 0.1$.

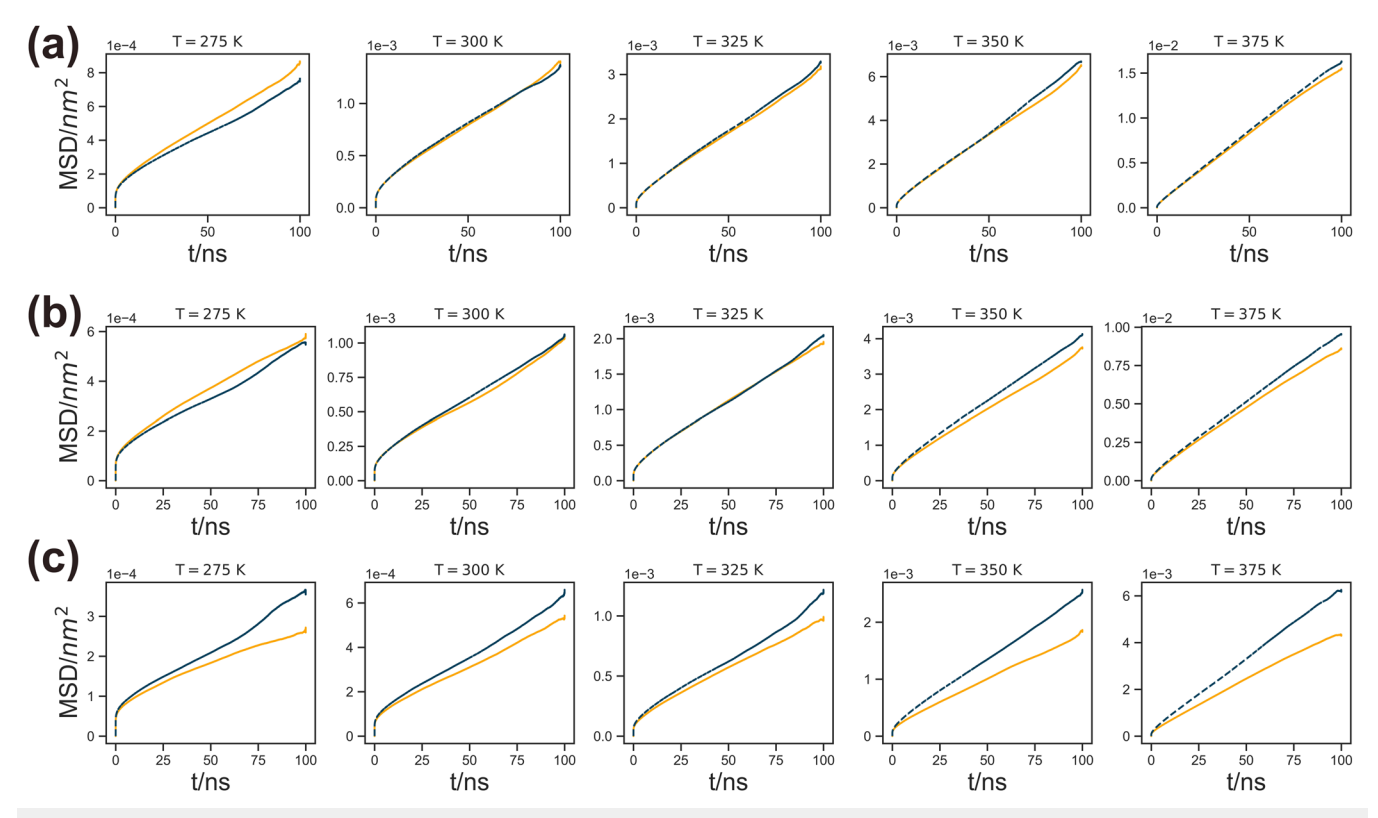


FIG. 18. Mean squared displacements for (a) BMP+, (b) TFSI-, and (c) Li+ as a function of temperature. The solid yellow lines represent the poly(MPC) ionogel, and the dashed blue line represents the base ILE.

chains indicative of "hopping". We observe that the hopping mechanism is a long timescale event that is interrupted by its association with the TFSI⁻. Type 2 Li⁺ is shown to be coordinated with both the polyZI and TFSI⁻ molecules. Type 3 Li⁺ coordination status is marked by the absence of the polyZI chain coordination along with the noticeable steep increase in the MSD. This is consistent with the relatively higher short-time sub-mean squared displacement of type 3 Li⁺ observed in Fig. 13(d). Overall, we can observe that Li⁺ travels via cyclic phases from associating exclusively to the polyZI chains to then coordinating with both TFSI⁻ and the polyZI chains and then to exclusive coordination with TFSI⁻.

3. Ion transport mechanisms: Discussion

In summary, from the concurrent analysis of MSD, poly(MPC) chain coordination status, and TFSI coordination status, we observed that type 1 Li⁺ travels via a "hopping" within the polymer matrix. Second, in our travel length analysis of Li⁺ associated with anions, we observed that type 2 Li⁺ travels via structural diffusion, while type 3 Li⁺ moves through a vehicular diffusion mechanism. Third, with increasing X_{ZI} , we observe the dominant Li⁺ ion transport of the poly(MPC) ionogel transitioning from vehicular to a structural transport mechanism. Furthermore, with increasing $X_{\rm ZI}$, we observe an increasing fraction of type 1 Li⁺ ions, which are shown above to travel via "hopping" mechanisms. Therefore, we anticipate an increased presence of "hopping" mechanism with increasing $X_{\rm ZI}$. Overall, we observe the ${\rm Li}^+$ ion transport mechanism in the poly(MPC) ionogel, which is a combination of hopping, structural, and vehicular mechanism, in contrast to the combination of only the vehicular and structural mechanism possible in Li-salt doped IL. We believe such differences may potentially explain the change in activation energy of conductivity observed in the experiments.

V. THE INFLUENCE OF TEMPERATURE

We recall that the experimental observations showed that the poly(MPC) ionogel displayed higher conductivity than the base ILE at room temperature. However, for T > 300 K, the conductivity trends were reversed. Our simulations were conducted at a high temperature of T = 600 K to obtain accurate statistics and were able to qualitatively reproduce the latter trends. To understand the temperature dependence and the origin of the crossover in the conductivities of the poly(MPC) ionogel and the base ILE at low temperatures, we performed molecular dynamics simulations at four other temperatures: 275, 300, 325, and 375 K using the annealing methodology detailed in the work of Abbott et al. 48 These simulations were conducted for both the poly(MPC) ionogel and its base ILE while keeping the salt concentration constant at $C_{L,i^+} = 0.5$ in accordance with the experimental setup. We calculated the mean squared displacement (MSD) for the mobile ions (Li⁺, BMP⁺, and TFSI⁻) in both the poly(MPC) ionogel and the base ILE. However, it was not possible to extract diffusivities and calculate the corresponding Nernst-Einstein conductivities at such low temperatures. As a result, we compared only the mean squared displacements of the ions in the poly(MPC) ionogel and its base ILE.

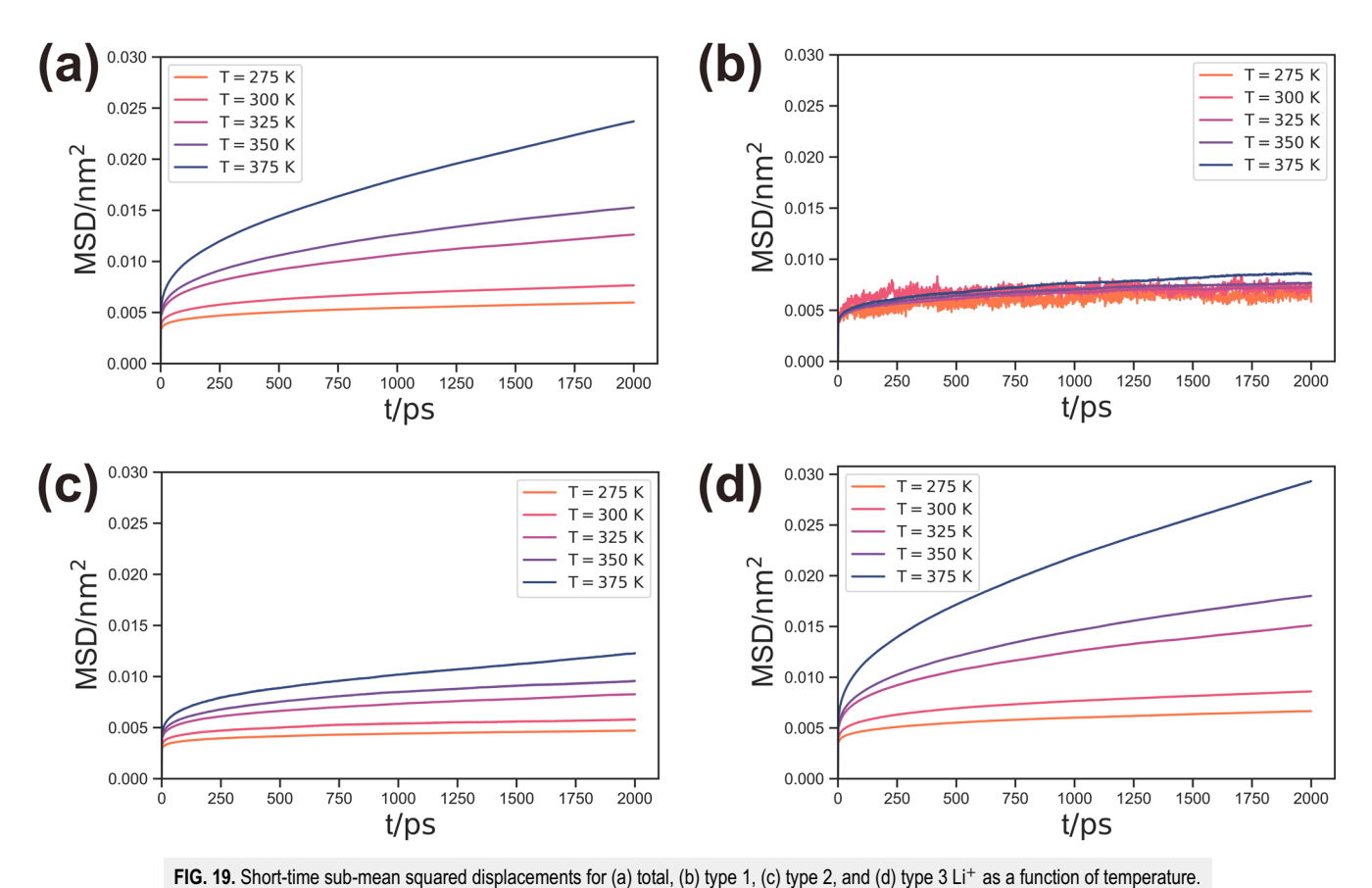
Figure 18 displays the mean squared displacement for (a) BMP⁺, (b) TFSI⁻, and (c) Li⁺ as a function of temperature. In Figs. 18(a) and 18(b), the MSD results of BMP⁺ and TFSI⁻, respectively, show a crossover in the relative values for poly(MPC) vs

base ILE at T = 300 K. Specifically, we observe that the dynamics of BMP⁺ and TFSI⁻ in the poly(MPC) ionogel is slightly faster than that in the base ionic liquid at T = 275 K. In contrast, for T > 300 K, we observe that the dynamics of BMP⁺ and TFSI⁻ in the poly(MPC) ionogel are slower than the corresponding base ILE. However, in Fig. 18(c), we observe that the dynamics of Li⁺ ions in the poly(MPC) ionogel are slower than its corresponding base ILE at all temperatures. We note that similar diffusivity trends have also been observed by Costa and co-workers⁴ in MD simulations of ZI oligomer ionogel-poly(2-methacryloyloxyethyl phosphorylcholine-co-sulfobetaine vinylimidazole) [poly(MPC-co-SBVI)]/1 M LiTFSI/BMPTFSI, which exhibits a similar conductivity trend crossover when compared to its base ILE in experiments as a function of temperature.¹⁹

Despite the lack of a crossover in MSDs of Li⁺ ions, we focus on analyzing the effects of temperature on the different categories of Li⁺ ions to indirectly understand its effects on the dynamics of BMP⁺ and TFSI⁻. Toward the said objective, we probed the shortterm sub-mean squared displacements for type 1, type 2, and type 3 Li⁺ as a function of temperature in Fig. 19. In Fig. 19(b), the type 1 Li⁺ and type 2 Li⁺ dynamics are observed to be minimally affected by the increasing temperature when compared to the changes in the dynamics of type 3 Li⁺ ions. Additionally, we note that the respective fractions type 1, type 2, and type 3 Li⁺ ions did not change as a function of temperature (Fig. S8 of the supplementary material). Overall, from the MSD analysis in Fig. 19, we observe that the different coordination types of Li+ are affected by temperature in the following order: type 3 » type 2 > type 1 Li⁺ ions. From this, we can infer that the dynamics of the mobile ions that are not associated with the poly(MPC) are influenced more strongly by variations in temperature.

As a result, we speculate that the crossover in conductivity between the poly(MPC) ionogel and the base ILE at lower temperatures arises from the influences of temperature on mobile ions, which are not associated with poly(MPC). This is consistent with the results of Figs. 18(a) and 18(b) in which the temperature variation was seen to be more likely to influence the dynamics of the base ionic liquid than the dynamics of the poly(MPC) ionogel. As we decrease the temperature, the mobility of the base ionic liquid will decline faster than the dynamics of the poly(MPC) ionogel. This will lead to having a lower conductivity of base ionic liquid than the poly(MPC) ionogel at lower temperatures.

We do note that our mean squared displacement of Li⁺ did not agree with the room temperature experimental results, such as the conductivity trend crossover as well as increased lithium transference number and Li⁺ diffusion coefficient. We hypothesize that this may also be a result from the method of polymerization implemented in the experiments. The poly(MPC) ionogel formulated by Panzer and co-workers is synthesized via in situ free radical polymerization of a well-mixed precursor solution containing LiTFSI, BMP TFSI, and MPC monomers.11 However, our simulations resemble the process of polymerizing the poly(MPC) separately and subsequently equilibrating it with a salt-doped IL solution. The blending of poly(MPC) with salt in the simulations may lead to a higher self-association of the poly(MPC) leading to fewer Li⁺ ions coordinating with the polyZI chains. This key difference in preparation may result in fewer type 1 Li⁺ ions in simulations relative to the experiments. Therefore, having fewer type 1 [Li]⁺



ions, which have been demonstrated to be less affected by temperature variations, may explain the absence of the ${\rm Li}^+$ MSD and ${\rm Li}^+$ diffusivity crossover observed in simulations as a function of temperature.

VI. CONCLUSIONS

In this article, we used atomistic molecular dynamic simulations to investigate the impact of polyZI content and salt concentration on the static and dynamic properties of poly(MPC) supported LiTFSI/BMP TFSI ILE (poly(MPC) ionogel). Additionally, we studied the ion transport mechanisms and the influence of temperature on the poly(MPC) ionogel. For increasing polyZI content (X_{ZI}) , our simulations indicated increased coordination of Li⁺, BMP⁺, and TFSI with the polyZI. As a result, we observed the disruption of Li^+ and TFSI⁻ interaction in the bulk ILE with increasing X_{ZI} . This was rationalized by the strong Li⁺-ZI[-] interaction observed in our simulations consistent with the experimental results. At higher $X_{\rm ZI}$, we also observed the increased coordination of BMP⁺ with the polyZI chains due to its secondary preferential association with the poly(MPC). With increasing X_{ZI} , we observed a decreasing mobility in all the mobile ions. Furthermore, the results showed a decrease in the Nernst-Einstein conductivity and lithium transference numbers.

This was rationalized by the fractions and dynamics of Li⁺ exclusively coordinated with the polyZI (type 1), Li⁺ ions coordinated with both TFSI⁻ and ZI[-] (type 2 Li⁺), and Li⁺ ions exclusively coordinated with the TFSI⁻ ions (type 3 Li⁺). The type 3 Li⁺ ions displayed faster dynamics than the dynamics of type 2 Li⁺ ions followed by the dynamics of type 1 ions. Furthermore, with increasing X_{ZI} , the results indicate increasing type 1 and type 2 Li⁺ ion fractions and decreasing type 3 Li⁺ ion fractions. Such coordination statistics and their corresponding dynamics were used to rationalize the decreasing diffusivity results observed in our simulations.

On the other hand, while increasing the salt concentration (C_{Li^+}) , our simulations showed the opposite trend observed when increasing X_{ZI} . More explicitly, increasing C_{Li^+} , our results showed the increased coordination of Li^+ ions with the bulk IL ions and a decreased coordination with the polyZI chains. Furthermore, with an increase in C_{Li^+} , we observed a decrease in $\text{Li}^+\text{-ZI}[-]$ interactions followed by an increase in $\text{Li}^+\text{-TFSI}^-$ interactions. When comparing the poly(MPC) ionogel with its base ILE as a function of increasing C_{Li^+} , we observe that the diffusivity of the poly(MPC) ionogel is lower than the corresponding diffusivity of the base ILE in accordance with the experimental results above room temperature. The conductivity and the lithium transference numbers of the poly(MPC) ionogel were also observed to be lower than its corresponding base ILE as a function of C_{Li^+} . These dynamic properties

were in accordance with the experimental observation at T > 300 K. Additionally, we observed a similar decreasing BMP⁺ and TFSI⁻ diffusivity trend. However, contrary to the base ILE, we observed an increasing Li+ diffusivity trend. This was again rationalized by the dynamics and fraction of type 1, type 2, and type 3 Li⁺ ions as a

In terms of identifying the ion transport mechanisms, our results demonstrated that type 1 Li+ ions primarily travel via a hopping "like" mechanism, type 2 Li+ ions predominantly move by structural diffusion, and type 3 Li⁺ ions mainly travel via a vehicular diffusion mechanism. The increase in X_{ZI} causes an increase in structural diffusion and a decrease in vehicular diffusion mechanism in the Li⁺ ions associated with the ions. Additionally, with an increase in X_{ZI} , we inherently increase the type 1 Li⁺ ion, which, in turn, increases the hopping "like" mechanisms present in the poly(MPC) ionogel. The opposite trend was observed when increasing C_{Li} +.

Finally, we demonstrated the influence of temperature on the mobile ions in poly(MPC) in comparison to the base ILE. Interestingly, our BMP⁺ and TFSI⁻ mean squared displacement (MSD) results captured the experimentally observed crossover of the conductivity trend between the poly(MPC) ionogels and the corresponding base ILEs, but the simulation Li⁺ MSD results did not agree with the experiment. We hypothesized that this resulted due to the difference in "preparation" between simulations and experiments. To indirectly understand the BMP+ and TFSI- dynamic trends, we demonstrated that the Li⁺ ions associated with the base ILE are influenced more than the Li+ ions associated with the polymer. Therefore, the conductivity crossover observed between the poly(MPC) ionogel and its base ILE was attributed to the higher influence of temperature on the dynamics of ions that are not associated with the poly(MPC) ionogels, thus resulting in the conductivity of the base ILE being lower than the poly(MPC) ionogel at low temperatures. Overall, the results of this study provide a fundamental understanding of polyZI ionogel, which we hope to further understand other chemistries of polyZIs and salts.

SUPPLEMENTARY MATERIAL

Electronic supplementary material is available. Section S1 shows the model and simulation details. Section S2 presents MD snapshots as a function of polymer and salt content. Section S3 presents the radial distribution function as a function of polymer and salt content. Sections S4 and S5 feature the influence of polymer content and salt concentration on BMP+ and TFSI- coordination statistics, respectively. Section S6 shows the influence of temperature on the coordination statistics of Li⁺ ions. Finally, Sec. S7 displays the linear fittings of the mean squared displacement for both the base ILE and poly(MPC) ionogel as a function of polymer and salt content.

ACKNOWLEDGMENTS

This work was generously supported by the Robert A. Welch Foundation (Grant No. F-1599) and the National Science Foundation (Grant No. DMR-2225167). The authors acknowledge the Texas Advanced Computing Center (TACC) for the generous allocation of computing resources. We thank Professor Matthew J. Panzer (Tufts University) for a number of insightful discussions.

AUTHOR DECLARATIONS

Conflict of Interest

The authors have no conflicts to disclose.

Author Contributions

Meron Y. Tadesse: Conceptualization (equal); Data curation (equal); Formal analysis (equal); Investigation (equal); Methodology (equal); Visualization (equal); Writing - original draft (equal); Writing - review & editing (equal). Zidan Zhang: Conceptualization (equal). Nico Marioni: Conceptualization (equal). Everett S. Zofchak: Conceptualization (equal). Tyler J. Duncan: Conceptualization (equal). Venkat Ganesan: Conceptualization (equal); Project administration (equal); Resources (equal); Writing – review & editing (equal).

DATA AVAILABILITY

The data that support the findings of this study are available from the corresponding author upon reasonable request.

REFERENCES

- ¹Energy demand: Three drivers, https://corporate.exxonmobil.com/energy-andinnovation/outlook-for-energy/energy-demand (accessed on 30 01 2023).
- ²S. Fleischmann, J. B. Mitchell, R. Wang, C. Zhan, D.-e. Jiang, V. Presser, and V. Augustyn, "Pseudocapacitance: From fundamental understanding to high power energy storage materials," Chem. Rev. 120, 6738-6782 (2020).
- ³W.-B. Li, D. Zhou, R. Xu, D.-W. Wang, J.-Z. Su, L.-X. Pang, W.-F. Liu, and G.-H. Chen, "BaTiO3-based multilayers with outstanding energy storage performance for high temperature capacitor applications," ACS Appl. Energy Mater. 2, 5499-5506 (2019).
- ⁴T. C Lourenço, M. Ebadi, M. J Panzer, D. Brandell, and L. T Costa, "A molecular dynamics study of a fully zwitterionic copolymer/ionic liquid-based electrolyte: Li⁺ transport mechanisms and ionic interactions," J. Comput. Chem. 42, 1689-1703 (2021).
- ⁵M. Watanabe, M. L. Thomas, S. Zhang, K. Ueno, T. Yasuda, and K. Dokko, "Application of ionic liquids to energy storage and conversion materials and devices," Chem. Rev. 117, 7190-7239 (2017).
- ⁶B. Diouf and R. Pode, "Potential of lithium-ion batteries in renewable energy," Renewable Energy 76, 375-380 (2015).
- ⁷W. Xu, J. Wang, F. Ding, X. Chen, E. Nasybulin, Y. Zhang, and J.-G. Zhang, "Lithium metal anodes for rechargeable batteries," Energy Environ. Sci. 7,
- ⁸Q. Wang, B. Liu, Y. Shen, J. Wu, Z. Zhao, C. Zhong, and W. Hu, "Confronting the challenges in lithium anodes for lithium metal batteries," Adv. Sci. 8, 2101111 (2021).
- ⁹Z. Lei, B. Chen, Y.-M. Koo, and D. R. MacFarlane, "Introduction: Ionic liquids," Chem. Rev. 117, 6633 (2017).
- ¹⁰B. E. Gurkan, J. C. de la Fuente, E. M. Mindrup, L. E. Ficke, B. F. Goodrich, E. A. Price, W. F. Schneider, and J. F. Brennecke, "Equimolar CO2 absorption by anion-functionalized ionic liquids," J. Am. Chem. Soc. 132, 2116-2117 (2010).
- ¹¹M. E. Taylor, D. Clarkson, S. G. Greenbaum, and M. J. Panzer, "Examining the impact of polyzwitterion chemistry on lithium ion transport in ionogel electrolytes," ACS Appl. Polym. Mater. 3, 2635-2645 (2021).

- 12 J. Wang, L. Xu, G. Jia, and J. Du, "Challenges and opportunities of ionic liquid electrolytes for rechargeable batteries," Cryst. Growth Des. 22, 5770-5784
- 13 A. Wu, F. Lu, P. Sun, X. Qiao, X. Gao, and L. Zheng, "Low-molecularweight supramolecular ionogel based on host-guest interaction," Langmuir 33, 13982-13989 (2017).
- ¹⁴A. S. Shaplov, R. Marcilla, and D. Mecerreyes, "Recent advances in innovative polymer electrolytes based on poly(ionic liquid)s," Electrochim. Acta 175, 18-34
- $^{15}\mathrm{V}.$ Ganesan, "Ion transport in polymeric ionic liquids: Recent developments and open questions," Mol. Syst. Des. Eng. 4, 280-293 (2019).
- 16Z. Zhang, E. Zofchak, J. Krajniak, and V. Ganesan, "Influence of polarizability on the structure, dynamic characteristics, and ion-transport mechanisms in
- polymeric ionic liquids," J. Phys. Chem. B. 126(13), 2583–2592 (2022). 17 Z. Zhang, D. Lin, and V. Ganesan, "Mechanisms of ion transport in lithium saltdoped polymeric ionic liquid electrolytes at higher salt concentrations," J. Polym. Sci. 60, 199-213 (2022).
- $^{18}\mbox{M.}$ E. Taylor and M. J. Panzer, "Fully-zwitterionic polymer-supported ionogel electrolytes featuring a hydrophobic ionic liquid," J. Phys. Chem. B 122, 8469-8476 (2018).
- ¹⁹ A. J. D'Angelo and M. J. Panzer, "Decoupling the ionic conductivity and elastic modulus of gel electrolytes: Fully zwitterionic copolymer scaffolds in lithium salt/ionic liquid solutions," Adv. Energy Mater. 8, 1801646 (2018).
- ²⁰ M. Yoshizawa, M. Hirao, K. Ito-Akita, and H. Ohno, "Ion conduction in zwitterionic-type molten salts and their polymers," J. Mater. Chem. 11, 1057-1062
- ²¹ N. Byrne, P. C. Howlett, D. R. MacFarlane, and M. Forsyth, "The zwitterion effect in ionic liquids: Towards practical rechargeable lithium-metal batteries," Adv. Mater. 17, 2497-2501 (2005).
- ²²J. R. Keith and V. Ganesan, "Ion transport mechanisms in salt-doped
- polymerized zwitterionic electrolytes," J. Polym. Sci. **58**, 578–588 (2020). ²³S. D. Jones, H. Nguyen, P. M. Richardson, Y.-Q. Chen, K. E. Wyckoff, C. J. Hawker, R. J. Clément, G. H. Fredrickson, and R. A. Segalman, "Design of polymeric zwitterionic solid electrolytes with superionic lithium transport," ACS Cent. Sci. 8, 169-175 (2022).
- ²⁴F. Lind, L. Rebollar, P. Bengani-Lutz, A. Asatekin, and M. J. Panzer, "Zwitterioncontaining ionogel electrolytes," Chem. Mater. 28, 8480-8483 (2016).
- ²⁵M. J. Abraham, T. Murtola, R. Schulz, S. Páll, J. C. Smith, B. Hess, and E. Lindahl, "GROMACS: High performance molecular simulations through multi-level parallelism from laptops to supercomputers," SoftwareX 1–2, 19–25 (2015). ²⁶ V. D. Spoel *et al.* (2021). "Gromacs 2020.5 source code," Zenodo.
- ²⁷W. L. Jorgensen, D. S. Maxwell, and J. Tirado-Rives, "Development and testing of the OPLS all-atom force field on conformational energetics and properties of organic liquids," J. Am. Chem. Soc. 118, 11225-11236 (1996).
- ²⁸W. L. Jorgensen and J. Tirado-Rives, "Potential energy functions for atomiclevel simulations of water and organic and biomolecular systems," Proc. Natl. Acad. Sci. U. S. A. 102, 6665-6670 (2005).
- ²⁹ J. N. Canongia Lopes and A. A. Pádua, "CL & P: A generic and systematic force field for ionic liquids modeling," Theor. Chem. Acc. 131, 1129-1211 (2012).
- ³⁰P. Bauer, B. Hess, and E. Lindahl (2022). "Gromacs 2022.1 manual," Zenodo, Preprint at https://doi.org/10.5281/ZENODO 6103568.

- ³¹ M. e. Frisch, G. Trucks, H. Schlegel, G. Scuseria, M. Robb, J. Cheeseman, G. Scalmani, V. Barone, G. Petersson, H. Nakatsuji et al., GAUSSIAN 16, revision c. 01, Gaussian, Inc., 2016.
- 32 C. I. Bayly, P. Cieplak, W. Cornell, and P. A. Kollman, "A well-behaved electrostatic potential based method using charge restraints for deriving atomic charges: The RESP model," J. Phys. Chem. 97, 10269-10280 (1993).
- ³³T. Lu and F. Chen, "Multiwfn: A multifunctional wavefunction analyzer," J. Comput. Chem. 33, 580-592 (2012).
- ³⁴L. Tian and C. Fei-Wu, "Comparison of computational methods for atomic charges," Acta Phys.-Chim. Sin. 28, 1-18 (2012).
- 35 A. A. Ribeiro, B. A. Horta, and R. B. d. Alencastro, "MKTOP: A program for automatic construction of molecular topologies," J. Braz. Chem. Soc. 19, 1433-1435 (2008).
- ³⁶G. S. Larsen, P. Lin, K. E. Hart, and C. M. Colina, "Molecular simulations of PIM-1-like polymers of intrinsic microporosity," Macromolecules 44, 6944-6951
- ³⁷R. W. Hockney, S. Goel, and J. Eastwood, "Quiet high-resolution computer models of a plasma," J. Comput. Phys. 14, 148-158 (1974).
- ${\bf ^{38}}$ T. Darden, D. York, and L. Pedersen "Particle mesh ewald: An n-log (n) method for ewald sums in large systems," J. Chem. Phys. 98 10089-10092 (1993); Mol. Phys. 52, 255-268 (1984).
- ³⁹G. Bussi, D. Donadio, and M. Parrinello, "Canonical sampling through velocity rescaling," J. Chem. Phys. 126, 014101 (2007).
- ⁴⁰M. Parrinello and A. Rahman, "Polymorphic transitions in single crystals: A new molecular dynamics method," J. Appl. Phys. 52, 7182-7190 (1981).
- $^{\mathbf{41}}\text{S.}$ Nosé and M. Klein, "Constant pressure molecular dynamics for molecular systems," Mol. Phys. 50, 1055-1076 (1983).
- ⁴²N. Marioni, Z. Zhang, E. S. Zofchak, H. S. Sachar, S. Kadulkar, B. D. Freeman, and V. Ganesan, "Impact of ion-ion correlated motion on salt transport in solvated ion exchange membranes," ACS Macro Lett. 11, 1258-1264 (2022).
- ⁴³F. Chen, P. Howlett, and M. Forsyth, "Na-ion solvation and high transference number in superconcentrated ionic liquid electrolytes: A theoretical approach," J. Phys. Chem. C 122, 105–114 (2018).
- ⁴⁴O. Borodin, G. D. Smith, and W. Henderson, "Li⁺ cation environment, transport, and mechanical properties of the LiTFSI doped N-methyl-Nalkylpyrrolidinium ⁺TFSI⁻ ionic liquids," J. Phys. Chem. B 110, 16879–16886 (2006).
- ⁴⁵J. B. Haskins, W. R. Bennett, J. J. Wu, D. M. Hernandez, O. Borodin, J. D. Monk, C. W. Bauschlicher, Jr., and J. W. Lawson, "Computational and experimental investigation of Li-doped ionic liquid electrolytes: [pyr14] [TFSI], [pyr13] [FSI], and [EMIM] [BF₄]," J. Phys. Chem. B 118, 11295–11309 (2014).
- ⁴⁶P. Nurnberg, E. I. Lozinskaya, A. S. Shaplov, and M. Schonhoff, "Li coordination of a novel asymmetric anion in ionic liquid-in-Li salt electrolytes," J. Phys. Chem. B 124, 861-870 (2020).
- ⁴⁷O. Borodin, G. A. Giffin, A. Moretti, J. B. Haskins, J. W. Lawson, W. A. Henderson, and S. Passerini, "Insights into the structure and transport of the lithium, sodium, magnesium, and zinc bis(trifluoromethansulfonyl)imide salts in ionic liquids," J. Phys. Chem. C 122, 20108-20121 (2018).
- ⁴⁸L. J. Abbott and A. L. Frischknecht, "Nanoscale structure and morphology of sulfonated polyphenylenes via atomistic simulations," Macromolecules 50, 1184-1192 (2017).